(2)

Defense Nuclear Agency
Alexandria, VA 22310-3398

DNA-TR-89-82

Radar Detection During Scintillation

D. L. Knepp
J. T. Reinking
Mission Research Corporation
P.O. Box 51203
Pacific Grove, CA 93950-6203

April 1990

Technical Report

CONTRACT No. DNA 001-87-C-0169

DISTRIBUTION LIST UPDATE

This mailer is provided to enable DNA to maintain current distribution lists for reports. We would appreciate your providing the requested information.

☐ Add the individual listed to your distribution list.

☐ Delete the cited organization/individual.

☐ Change of address.

NAME: _____

ORGANIZATION: _____

OLD ADDRESS	CURRENT ADDRESS
_____	_____
_____	_____
_____	_____

TELEPHONE NUMBER: ( ) _____

SUBJECT AREA(s) OF INTEREST:

_____ _____

_____ _____

_____ _____

DNA OR OTHER GOVERNMENT CONTRACT NUMBER: _____

CERTIFICATION OF NEED-TO-KNOW BY GOVERNMENT SPONSOR (if other than DNA):

SPONSORING ORGANIZATION: _____

CONTRACTING OFFICER OR REPRESENTATIVE: _____

SIGNATURE: _____

CUT HERE AND RETURN

Director
Defense Nuclear Agency
ATTN: TITL
Washington, DC 20305-1000

Director
Defense Nuclear Agency
ATTN: TITL
Washington, DC 20305-1000

REPORT DOCUMENTATION PAGE

Form Approved
OMB No. 0704-0188

1. AGENCY USE ONLY (Leave blank)	2. REPORT DATE	3. REPORT TYPE AND DATES COVERED
	900401	Technical 880101 - 881231

4. TITLE AND SUBTITLE

Radar Detection During Scintillation

5. FUNDING NUMBERS

C - DNA 001-87-C-0169
PE - 62715H
PR - RB
TA - RB
WU - DH039580

6. AUTHOR(S)

Dennis L. Knepp; J. Todd Reinking

7. PERFORMING ORGANIZATION NAME(S) AND ADDRESS(ES)

Mission Research Corporation
P. O. Box 51203
Pacific Grove, CA 93950-6203

8. PERFORMING ORGANIZATION REPORT NUMBER

MRC/MRY-R-015

9. SPONSORING/MONITORING AGENCY NAME(S) AND ADDRESS(ES)

Defense Nuclear Agency
6801 Telegraph Road
Alexandria, VA 22310-3398
RAAE/SCHROCK

10. SPONSORING/MONITORING AGENCY REPORT NUMBER

DNA-TR-89-82

11. SUPPLEMENTARY NOTES

This work was sponsored by the Defense Nuclear Agency under RDT&E RMC Codes B3200E4662DRBRB0014025904D and B3200A4662DRBRB0014025904D.

12a. DISTRIBUTION/AVAILABILITY STATEMENT

Approved for public release; distribution is unlimited.

12b. DISTRIBUTION CODE

13. ABSTRACT

Electromagnetic signals that propagate through a disturbed region of the ionosphere can experience scattering which can cause fluctuations in the received amplitude, phase, and angle-of-arrival. This report considers the performance of a radar that must operate through a disturbed propagation environment such as might occur during strong equatorial scintillation, during a barium release experiment or after a high altitude nuclear detonation. The severity of the channel disturbance is taken to range from weak scattering to the most severe case of strong scattering where the signal quadrature components are uncorrelated Gaussian variates. The detection performance of noncoherent combining is compared to that of double threshold (M out of N) combining under various levels of scintillation disturbance. Results are given for detection sensitivity as a function of the scintillation index and the ratio of the radar hopping bandwidth to the channel bandwidth. It is shown that both types of combining can provide mitigation of fading, and that noncoherent combining generally enjoys an advantage in detection sensitivity of about 2 dB. This work serves as a quantitative guideline to the advantages and disadvantages of certain types of detection strategies during scintillation and is, therefore, useful in the radar design process. However, a detailed simulation of the radar detection algorithms is necessary to evaluate a radar design strategy to predict performance under scintillation conditions.

14. SUBJECT TERMS

Frequency Hopping
Double-Threshold Detection
Ground Based Radar
Nuclear Effects
Scintillation
Noncoherent Detection
Space Radar
Fading

15. NUMBER OF PAGES
64

16. PRICE CODE

17. SECURITY CLASSIFICATION OF REPORT	18. SECURITY CLASSIFICATION OF THIS PAGE	19. SECURITY CLASSIFICATION OF ABSTRACT	20. LIMITATION OF ABSTRACT
UNCLASSIFIED	UNCLASSIFIED	UNCLASSIFIED	SAR

PREFACE

The authors wish to acknowledge many useful discussions regarding this work with Dr. G. A. Andrews of the Naval Research Laboratory. This work was supported by the Defense Nuclear Agency under Contract No. DNA 001-87-C-0169 and by the Naval Research Laboratory under Contract No. N00014-87-C-2336.

CONVERSION TABLE

Conversion factors for U.S. Customary to metric (SI) units of measurement

MULTIPLY → / TO GET ←	BY → / BY ←	TO GET / MULTIPLY
angstrom	1.000000 x E -10	meters (m)
atmosphere (normal)	1.01325 x E +2	kilo pascal (kPa)
bar	1.000000 x E +2	kilo pascal (kPa)
barn	1.000000 x E -28	meter^2 (m^2)
British thermal unit (thermochemical)	1.054350 x E +3	joule (J)
calorie (thermochemical)	4.184000	joule (J)
cal (thermochemical) / cm^2	4.184000 x E -2	mega joule/m^2 (MJ/m^2)
curie	3.700000 x E +1	*giga becquerel (GBq)
degree (angle)	1.745329 x E -2	radian (rad)
degree Farenheit	$(t_K=t_F+459.67)/1.8$	degree kelvin (K)
electron volt	1.60219 x E -19	joule (J)
erg	1.000000 x E -7	joule (J)
erg/second	1.000000 x E -7	watt (W)
foot	3.048000 x E -1	meter (m)
foot-pound-force	1.355818	joule (J)
gallon (U.S. liquid)	3.785412 x E -3	meter^3 (m^3)
inch	2.540000 x E -2	meter (m)
jerk	1.000000 x E +9	joule (J)
joule/kilogram (J/kg) (radiation dose absorbed)	1.000000	Gray (Gy)
kilotons	4.183	terajoules
kip (1000 lbf)	4.448222 x E +3	newton (N)
kip/inch^2 (ksi)	6.894757 x E +3	kilo pascal (kPa)
ktap	1.000000 x E +2	newton-second/m^2 (N-s/m^2)
micron	1.000000 x E -6	meter (m)
mil	2.540000 x E -5	meter (m)
mile(international)	1.609344 x E +3	meter (m)
ounce	2.834952 x E -2	kilogram (kg)
pound-force (lbs avoirdupois)	4.448222	newton (N)
pound-force inch	1.129848 x E -1	newton-meter (N.m)
pound-force/inch	1.751268 x E +2	newton/meter (N/m)
pound-force/foot^2	4.788026 x E -2	kilo pascal (kPa)
pound-force/inch^2 (psi)	6.894757	kilo pascal (kPa)
pound-mass (lbm avoirdupois)	4.535924 x E -1	kilogram (kg)
pound-mass-foot^2 (moment of inertia)	4.214011 x E -2	kilogram-meter^2 (kg m^2)
pound-mass/foot^3	1.601846 x E +1	kilogram/meter^3 (kg/m^3)
rad (radiation dose absorbed)	1.000000 x E -2	**Gray (Gy)
roentgen	2.579760 x E -4	coulomb/kilogram (C/kg)
shake	1.000000 x E -8	second (s)
slug	1.459390 x E +1	kilogram (kg)
torr (mm Hg, 0° C)	1.333220 x E -1	kilo pascal (kPa)

*The becquerel (Bq) is the SI unit of radioactivity; 1 Bq = 1 event/s.
**The Gray (Gy) is the SI unit of absorbed radiation.

TABLE OF CONTENTS

TABLE OF CONTENTS (Continued)

LIST OF ILLUSTRATIONS

LIST OF ILLUSTRATIONS (Continued)

LIST OF ILLUSTRATIONS (Continued)

SECTION 1

INTRODUCTION

The natural ionosphere can produce a variety of disturbances to radar signal propagation. Disturbances due to mean or very large-scale ionization include attenuation, phase shift, time delay, dispersion, polarization rotation, refraction, and multi-path. In addition, relatively small-scale ionospheric structure in the propagation medium can cause signal scintillation-essentially random fluctuations in the received signal phase, amplitude, angle-of-arrival and other signal properties. The effects of mean propagation disturbances have been the subject of many studies [*Budden*, 1985; *Lawrence, et al.*, 1964] and are well known. The effects of scintillation on the detection performance of space based radar are the subject of this report.

Electron density structure in the natural ionosphere can produce random variations in the amplitude and phase of a propagating wave, even at frequencies in the gigahertz range [*Skinner, et al.*, 1971; *Taur*, 1976]. These rapid variations in signal amplitude, phase, and angle-of-arrival are called scintillations and are often observed over satellite links through the ambient ionosphere at VHF and UHF [*Fremouw et al.*, 1978]. Radar measurements taken with the ALTAIR radar in the Pacific Test Range are known to give severely disturbed scintillation at 156 and 415 MHz [*Towle*, 1980]. Strong scintillation is occasionally observed at frequencies as high as C-band [*Franke, et al.*, 1984]. Since even small fluctuations in the received signal can degrade performance, the effect of scintillation must be considered in the design of a space based radar system intended to operate through an ionospheric channel.

The severity of the fluctuations depends upon the irregularity of the ionization structure and on the radar geometry and frequency. If the propagation environment is highly disturbed and the radar frequency not sufficiently high, worst-case scintillation may occur wherein the received signal quadrature components are uncorrelated Gaussian variates, after one-way propagation over the severely disturbed path. Worst-case, i.e., Rayleigh amplitude, scintillation is likely to occur if the ionosphere is highly disturbed, as for example by high altitude nuclear explosions [*Arendt and Soicher*, 1964; *King and Fleming*, 1980] or by chemical releases [*Wolcott, et al.*, 1978]. An increase in the radar frequency or a lessening of the ionization irregularity can lead to a decreased disturbance in the received signal with a corresponding change in the signal statistical description. In general, however, a signal at one frequency (or time) may show some statistical correlation to a signal received at a different frequency (or

time). The effects of signal decorrelation with time and frequency at all levels of scintillation severity are important to any UHF through X-band radar system that must operate through an ambient or disturbed ionospheric channel.

Previous authors [*Schwartz*, 1956; *Linder and Swerling*, 1956; *Walker*, 1971] have studied the performance of M out of N radar detection for the case of an undisturbed propagation channel. In an earlier work [*Dana and Knepp*, 1983], the impact of strong (Rayleigh) fading on radar noncoherent detection performance was reported, assuming various radar geometries and target models. The effects of frequency correlation were also studied in this work, however, the method used to model frequency correlation was limited to a single coherence function.

The effects of scintillation on monostatic radar employing "double-threshold" (M out of N) detection or noncoherent integration are the subjects of this work. (In general, noncoherent integration provides superior performance; however, double-threshold detection is of interest since it affords a radar design simplification.) In particular, methods are developed to study the effects of varying levels of scintillation on the probability of detecting targets of constant cross section as well as targets whose cross section follows the Swerling II model. In addition, simulation methods are developed to study the effects on probability of detection of correlation of the propagation channel over time and frequency.

This report utilizes the Nakagami-m probability distribution [*Nakagami*, 1960] to describe the statistics of the received signal power for the monostatic radar geometry. This simple, one-parameter distribution correctly describes both the weak and strong scattering limits of the actual probability distribution of scintillation [*Knepp and Valley*, 1978] and has been found to give a very good fit to observed scintillation data [*Fremouw, et al.*, 1980] over a wide range of scintillation conditions. The Nakagami-m distribution, as used here, permits the study of radar performance over the entire range of possible scintillation conditions.

When the two extreme assumptions on correlation of propagation effects are made (i.e., receive signal statistics due to propagation fluctuations for different bursts within a look are either independent or else completely correlated), then expressions may be developed for detection probability which are readily evaluated via numerical methods. For the case of partially correlated bursts, Monte Carlo methods are required to determine the effect on probability of detection. The simulation methods developed here allow a completely general specification of burst-to-burst correlation and may be used to study the effects of scintillation on the performance of frequency agile radar.

In this report a coherent pulse train is referred to as a burst, and a number of bursts that are combined noncoherently in some fashion is called a look. It is assumed that there is no signal decorrelation over the duration of a burst and, therefore, no coherent integration loss [*Dana and Knepp*, 1983].

1.1 IONIZATION IRREGULARITY DESCRIPTION.

Figure 1 depicts the geographic distribution of ionospheric scintillation as it is currently known [*Aarons*, 1975]. The severity of the scintillation is indicated in the figure by the density of the cross-hatching. Most severe ionization irregularities occur in a geographic region of about 20 degrees of latitude north and south of the geomagnetic equator. Equatorial scintillation is observed during a period of approximately 8 PM local time to about 2 AM and may regularly take the form of saturated Rayleigh amplitude fading at VHF and UHF, and occasionally at L-band. Equatorial scintillation is known to be more severe than mid- or high-latitude scintillation.

At high latitudes, scintillation occurs within the auroral region and over the polar cap. At present the occurrence of auroral scintillation is less understood than equatorial scintillation. However, it is known that auroral scintillation is more irregular than equatorial scintillation and can occur anytime during the local day or night. Increased magnetic activity brings higher levels of scintillation and can cause changes in the location of scintillation boundaries at high latitudes. The severity of scintillation can be measured by the S_4 scintillation index which characterizes the depth of fading.

An example of the hourly and seasonal distribution of amplitude scintillation is shown in Figure 2 [*Hawkins and Mullen*, 1974] in terms of average contours of the AFGL SI scintillation index. This measurement of scintillation severity can easily be obtained from strip charts. The innermost contour shown corresponds to a value of SI of 70 or roughly to a value of S_4 of 0.36 signifying 8 dB peak-to-peak fading. This data was obtained from an accumulation of six years of observations of ATS-3 from Huancayo, Peru. The figure shows that scintillation at this location is most severe during the months of February through October and during the hours immediately preceding local midnight. Similar measurements from other geographic locations indicate the presence of a longitudinal dependence on seasonal scintillation activity. Although average results of this type are extremely useful they are insufficient to design an SBR to operate during signal scintillation. SBR design and evaluation are best served with measurements of the distribution function of S_4 so that the designer can determine the percentage of time peak-to-peak signal fluctuations of a certain level are exceeded.

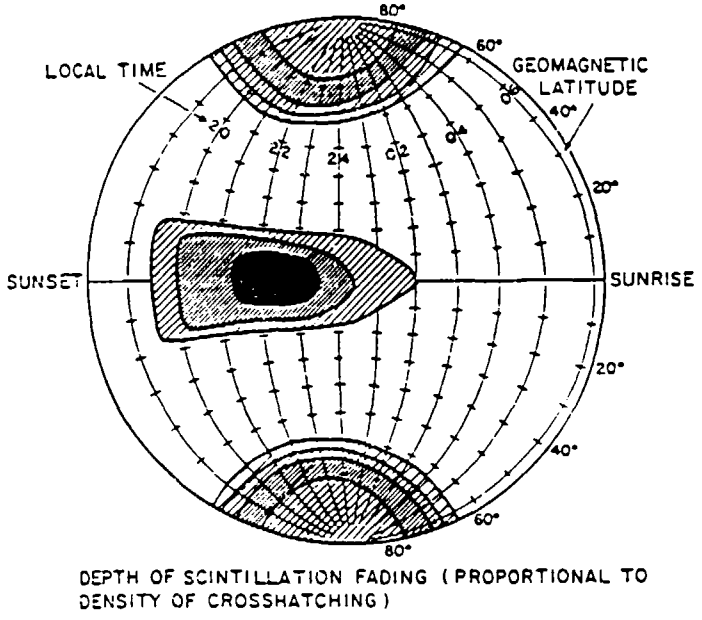

Figure 1. Geographic distribution of ionospheric fading.

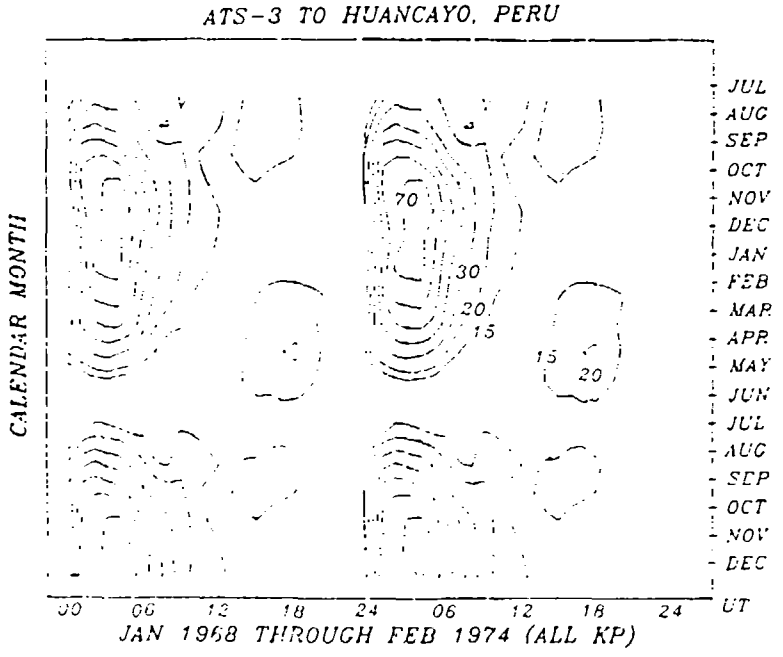

Figure 2. Average scintillation (SI) contours at 136 MHz obtained over a six year period. Universal time shown is 5 hours less than local time (05 UT is 24 LT).

The DNA Wideband satellite experiment has assembled the most extensive collection of phase coherent scintillation data to date [*Fremouw et al.*, 1978]. Figure 3 [*Livingston*, 1978] shows the seasonal dependence of scintillation at 137 MHz as measured during Wideband passes observed from Ancon, Peru. The Wideband orbit is sun-synchronous so that the satellite always passes over the equator at a constant local time of about 11:30 PM. Thus from a fixed ground location, three or four passes are observable each night of operation. In addition, each pass takes about 15 minutes. For the purposes of data analysis this time period is divided into many 10 second segments. The S_4 scintillation index is obtained once for each 10 second segment giving many measurements of S_4 during the night. Figure 3 shows the percentage of measurements of S_4 at Ancon where the value of 0.3 was exceeded at 137 MHz. This value corresponds to about 6 dB peak-to-peak fading.

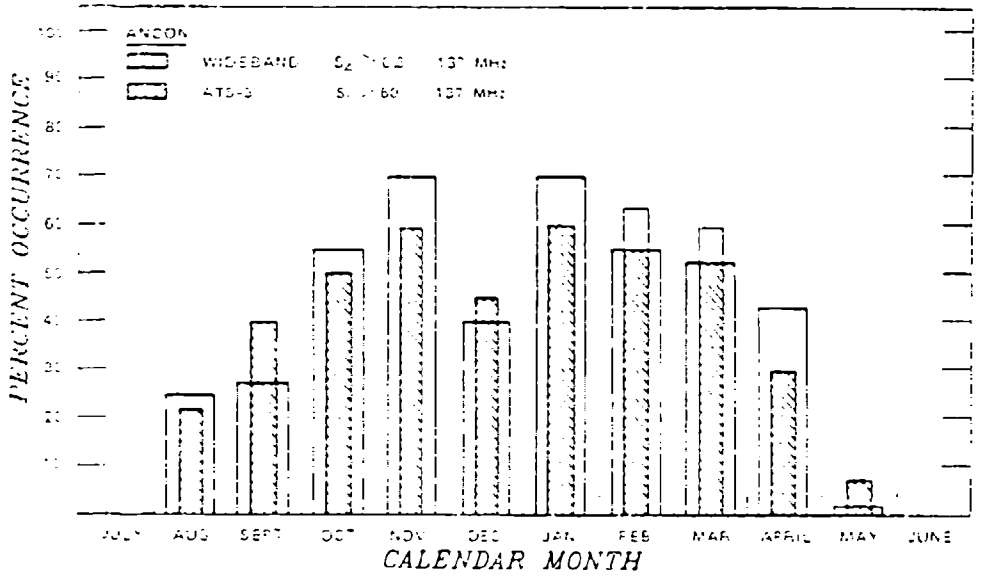

Figure 3. Seasonal dependence of scintillation severity at Ancon, Peru.

Values of scintillation index depend on geometry, frequency, and the ionization irregularity structure. Results from the DNA Wideband satellite are very appropriate for the design of systems that might use high inclination orbits since the Wideband satellite was in an almost polar orbit at an altitude of 1000 km. Therefore these measurements may be used directly for satellites in similar orbits, but need to be scaled to apply to different radar transmission frequencies and satellite altitudes.

Figures 4 and 5 [*Knepp*, 1978] show Wideband data taken on a particularly severe pass over Ancon, Peru on December 16, 1976. Figure 4 shows values of the S_4 scintillation index obtained at 138, 379 and 447 MHz during a brief portion of a satellite pass. In this study a measurement of S_4 is obtained by averaging over each 10.5 seconds of data giving sixteen measurements at each of the three frequencies during the 2.8 minute time period shown. During the beginning of this period propagation conditions were quite severe with worst case Rayleigh fading (unity S_4) observed at VHF and the two UHF frequencies shown. However a few minutes later, the scintillation severity is observed to decrease somewhat with very little scintillation (small S_4) at UHF at 23:51 although at VHF scintillation is still severe.

Figure 5 shows values of the cross-correlation function of the received intensity or power as obtained from the first six 10.5 second intervals shown in the previous figure. The cross-correlation coefficient is shown for correlations between the lowest Wideband UHF tone at 379 MHz and the tones at 390, 413, 436 and 447 MHz. From the figure it is evident that the tones are well decorrelated for the two earliest measurements at 23:48:29 and 23:48:50 for the 379-413 MHz frequency pair. For later times during this Wideband pass the UHF frequency tones become well correlated across the spectrum from 379 to 447 MHz as shown by the curve at 23:49:11. The data here show an example where the tones at 379 and 413 MHz were decorrelated. The coherence bandwidth is proportional to transmission frequency to the fourth power so that if this 34 MHz frequency separation were scaled to apply to a VHF radar at 200 MHz, the resulting coherence bandwidth would be about 4 MHz. Thus during the scintillation conditions observed during these measurements, the propagation channel would effectively decorrelate for VHF frequencies separated by more than 4 MHz. A good radar design could take advantage of this decorrelation with transmission frequency by noncoherently combining the radar returns from independent samples of the fading channel.

The mechanisms accounting for irregularity production have been the subject of many research papers over the last decade and are now reasonably well understood [*Keskinen and Ossakow*, 1981; *Tsunoda*, 1988]. In the equatorial regions the dominant mechanism for production of large scale structure or equatorial spread-F is the collisional Rayleigh-Taylor instability. The emerging view is that high-latitude irregularities in electron density are produced primarily by the gradient-drift (or $\bar{E} \times \bar{B}$) instability.

Although other forms have been observed, the power spectral density of the electron-density structure is well represented by a two-component power-law form with the irregularities highly elongated along the direction of the earth's magnetic field. The precise values of the parameters that describe the spectrum are under

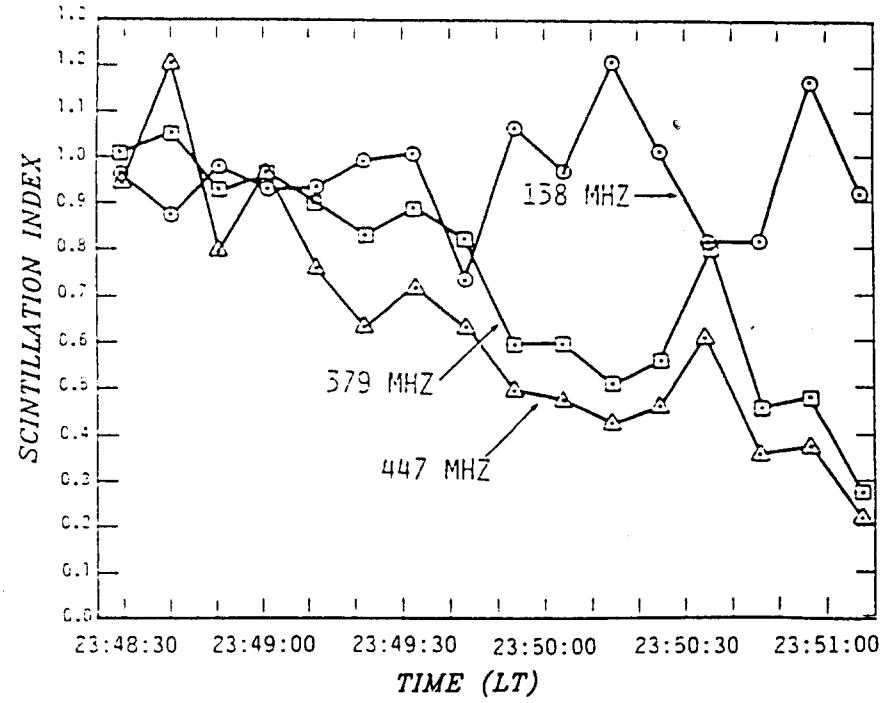

Figure 4. Simultaneous VHF and UHF scintillation observed during the DNA Wideband satellite experiment.

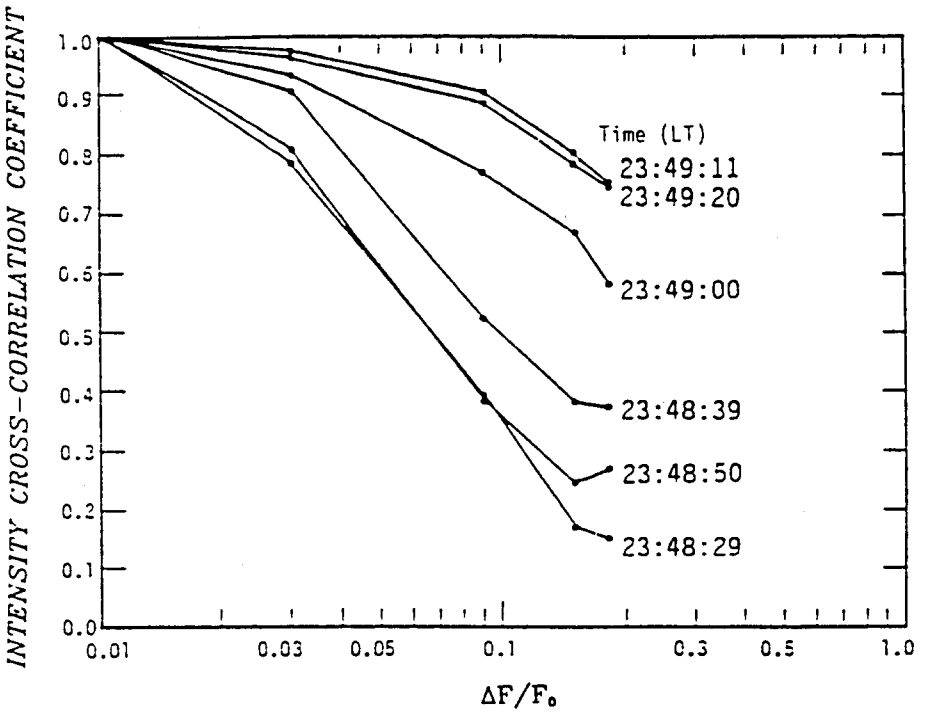

Figure 5. Cross-correlation of power at different UHF frequencies during the DNA Wideband satellite experiment.

current investigation by a number of researchers. However, the current belief is that the spectrum behaves as K^{-4} for spatial wavenumbers (K) greater than the freezing scale and flattens to between $K^{-2.3}$ and $K^{-2.7}$ for scale sizes ranging from the freezing scale to the outer scale. The outer scale ranges from 10-100 km and the freezing scale ranges from 150-1000 m. One view of the irregularity structure causing scintillation is a thick layer (~200 kilometers) extending upwards from the base of the F-region and having electron density fluctuations on the order of 50-100 percent of the mean electron density [*Basu and Basu*, 1976].

SECTION 2

RECEIVED SIGNAL DESCRIPTION

If the radar signal passes through a disturbed propagation channel subject to electron density irregularities, the received signal amplitude may experience fluctuations or scintillation. Knowledge of the probability distribution of the received signal is essential to determine radar system performance. Since the 1950s, many authors have investigated the probability distribution of the received signal after one-way propagation through turbulence [*Knepp and Valley*, 1978 and references therein]. A large number of probability distribution functions that describe various aspects of the received scintillated signal are possible. Many distributions correctly describe the weak-scattering regime, and parametrically extend to the strong-scattering limit. The joint Gaussian distribution is generally the most useful to describe higher moments of the received electromagnetic field. However, in a definitive paper *Fremouw, et al.* [1980] utilized measurements to show that the Nakagami-m distribution is clearly superior to the log-normal, the generalized Gaussian and the two-component Gaussian distribution to describe the probability density function of the received power for the case of radio wave scattering. This conclusion is based on a comprehensive analysis of the large body of multi-spectral scintillation data collected during the DNA Wideband Satellite experiment.

2.1 RECEIVED SIGNAL FIRST-ORDER STATISTICS.

In fading conditions it is convenient to write the received signal power as [*Dana and Knepp*, 1983]

$$S_r = S_0 S\sigma/\langle\sigma\rangle \tag{1}$$

In this expression for the received power, S_0 is the mean signal power received from the target, S is the fractional change in the signal power due to variations caused by the propagation channel, and $\sigma/\langle\sigma\rangle$ is the fractional change in the signal power caused by target cross section fluctuations. The factor S_0 contains the mean signal level; therefore, the mean value $\langle S\rangle$ is unity. Since the mean signal level has no statistical variation, the received signal power fluctuations can be expressed as the product of the effects of fluctuations due to propagation disturbances and to target variations.

2.2 TARGET STATISTICS.

Consider the case of a radar that transmits bursts that are separated by a large amount of time relative to the decorrelation time of the target cross section variations. A similar situation arises for the case that the radar transmission frequency is changed sufficiently from burst to burst, so that the target cross section is decorrelated from burst to burst. In either case the target cross section variation can often be assumed to be described by a Swerling II model. A Swerling II model applies to the case that the cross section varies independently from burst to burst. This nomenclature differs from the original Swerling II convention only in the replacement of Swerling's "pulse" by a "burst" in this work. The probability density function for target cross section variation is given by the expression

$$p(\sigma) = \frac{1}{\langle\sigma\rangle} \exp(-\sigma/\langle\sigma\rangle), \quad \sigma \geq 0 \tag{2}$$

where $\langle\sigma\rangle$ is the mean value. The angle brackets denote a stochastic average. Since a target with constant cross section is also of interest to certain defense radars, results are also included for this case.

2.3 PROPAGATION CHANNEL STATISTICS.

To completely characterize the first-order statistics at the radar receiver, the statistics of the signal fluctuations caused by propagation through a disturbed channel are required. Using Nakagami-m statistics the probability density function of fading on the one-way propagation channel is controlled by the m-parameter defined by the equation

$$\frac{1}{m} = S_4^2 = \frac{\langle (P - \langle P\rangle)^2\rangle}{\langle P\rangle^2} \tag{3}$$

In this equation S_4 is referred to as the scintillation index and is a measure of the severity of the fluctuations of power. The quantity P is the received power on a one-way propagation path. The S_4 index is thus the normalized standard deviation of the received power on a one-way propagation path where the transmitted power is constant. Values of S_4 generally range from a minimum of zero signifying constant power or no scintillation to a maximum of unity indicating worst-case (Rayleigh)

fading of amplitude where the in-phase and quadrature components of the received one-way signal are uncorrelated Gaussian variates. Values of S_4 greater than unity have been observed, but these indicate the presence of signal enhancements due to focusing. Since S_4 has been used more frequently in the past to describe scintillation, it will be used to quantify the scintillation severity in place of m in the remainder of this report.

For a one-way propagation path the probability density function of received power is given by [*Nakagami*, 1960]

$$p_1(S) = \frac{m^m S^{m-1}}{\Gamma(m)\langle S\rangle^m} \exp\left\{\frac{-mS}{\langle S\rangle}\right\}, \quad S \geq 0, \text{ one-way} \tag{4}$$

where the subscript refers to the one-way propagation path. For the case of monostatic radar operation, the transmitter and receiver are collocated so the signal propagates twice over the same path, passing through identical irregularities. In this case the received voltage is proportional to the square of the voltage after one-way propagation [*Knepp*, 1985]. The probability density function for the received power may be obtained from Equation 4 using the transformation $Q(\text{monostatic}) = S^2(\text{one-way})$ with the result

$$p_2(Q) = \frac{[m(m+1)]^{m/2} Q^{m/2-1}}{2\Gamma(m)\langle Q\rangle^{m/2}} \exp\left\{-\sqrt{\frac{m(m+1)Q}{\langle Q\rangle}}\right\}, Q \geq 0, \text{ two-way} \tag{5}$$

Note that the Nakagami-m density is a generalization of the chi-square probability density function. The chi-square density can be obtained from Equation 4 by replacing the m-parameter with $n/2$ and performing the change of variable $y = nS$ on the resulting equation. In the resulting equation, y is the chi-square variate and n is the number of degrees of freedom which is restricted to positive integer values.

It is straightforward to compute the relationship between the value of S_4 measured on the monostatic radar, two-way path as a function of m on the one-way path as $S_4^2(\text{two-way}) = (4m^2+10m+6)/(m(m+1)^2)$. Thus, under Rayleigh statistics, the maximum value of S_4 on the two-way path, corresponding to a monostatic radar geometry, is $\sqrt{5}$. Figure 6 shows the cumulative distribution of the received power on a round trip propagation path that characterizes a monostatic radar geometry consisting of two one-way propagation paths. The cumulative distribution is shown as a function of the value of S_4 on each one-way propagation path. For worst-case scintillation in

the monostatic radar geometry it is seen from the figure that the probability of a 10 dB fade or greater is about 40 percent. This high probability of fading is reflected in degradation of various aspects of radar performance including reduced radar target detection performance.

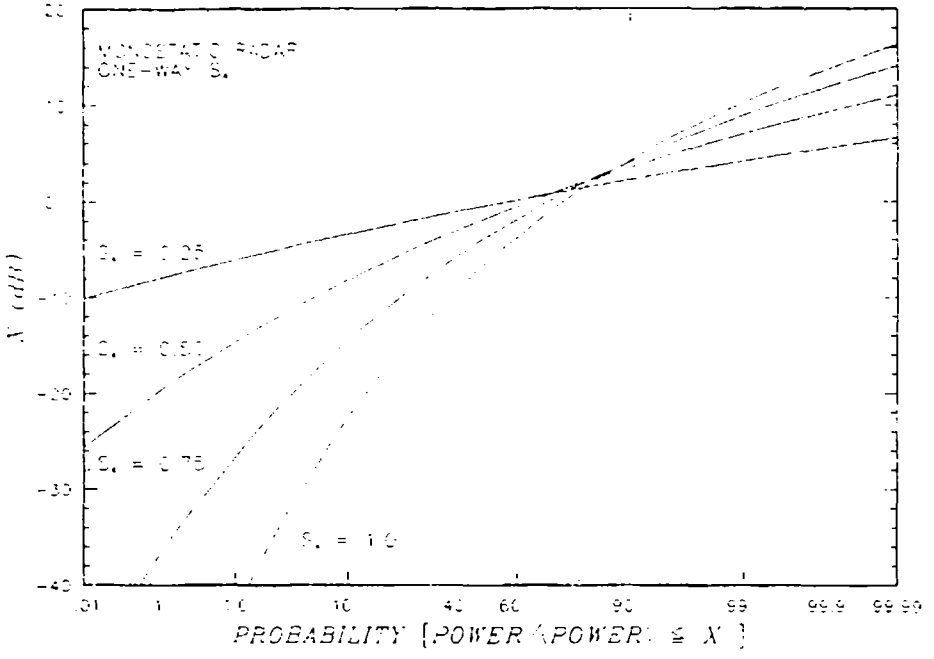

Figure 6. Cumulative probability distribution of received two-way power as a function of S_4 on the one-way propagation path.

2.4 PROPAGATION CHANNEL COHERENCE.

The above discussion fully describes the first-order power statistics to be expected after propagation of a radar signal through a disturbed ionospheric channel.

The second-order fading statistics are specified by the correlation function of the received complex voltage. For the case of one-way propagation of an initially constant amplitude signal through a severely disturbed ionospheric channel, the auto-correlation function of the received voltage is given as the two-position, two-frequency mutual coherence function. The effective velocity of the line of sight of the radar signal through the ionospheric irregularities can be utilized to convert the spatial coordinates

of the mutual coherence function into temporal coordinates and thereby obtain the correlation function of signal fluctuations due to ionospheric irregularities.

For worst-case Rayleigh fading, the correlation function of the received complex voltage $E(t, f)$ has the form

$$\langle E(t+\tau, f+f_d)E^*(t,f)\rangle = |E_0|^2 \exp\left\{\frac{-\tau^2/\tau_0^2}{1+if_d/f_{coh}}\right\}(1+if_d/f_{coh})^{-1} \qquad (6)$$

where τ_0 is the decorrelation time (the fading rate is $1/\tau_0$) for fluctuations over a one-way propagation path. The actual value of τ_0 is a function of radar geometry and of the irregularity structure and intensity of the disturbed ionospheric channel. Large values of τ_0 correspond to slow fading conditions and small values correspond to fast fading.

As a concrete example, consider the case of a radar and target separated by a layer of ionization as might occur in the case of an SBR observing a target near the ground. For a K^{-4} in situ power spectrum of three-dimensional ionization irregularities between outer scale L_0 and inner scale l_i, the decorrelation time is

$$\tau_0 = \sqrt{2}L_0/\sqrt{ln(L_0/l_i)}\sigma_\phi v_L \qquad (7)$$

where v_L is the velocity of the line of sight through the center of the ionized layer, σ_ϕ^2 is $2(r_e\lambda)^2 L_0 L\overline{\Delta N_e^2}$ rad^2, λ is the RF wavelength, r_e is the classical electron radius (2.82 $\times$ 10^{-15} m), L is the thickness of ionized layer, and $\overline{\Delta N_e^2}$ is the variance of electron density irregularities.

It is assumed that τ_0 is large with respect to the duration of the transmitted pulse. The received signal is then coherent during the pulse duration that is typically of the order of several tens of microseconds.

The channel coherence bandwidth is a measure of the maximum bandwidth available in the propagation channel over which it is possible to transmit a signal without undesired pulse distortion. That is, in a fading environment, signal spectral components separated by less than the coherence bandwidth exhibit correlated fluctuations. If the signal spectral components are separated in frequency by an amount greater than the coherence bandwidth, different spectral components will undergo uncorrelated fading. This distortion in the received signal spectrum causes the received time domain signal to display undesired time sidelobes. On the other hand, a

propagating pulse remains undistorted as long as the maximum instantaneous signal bandwidth is less than the coherence bandwidth. This is often the case for frequency-agile radar systems. In addition, frequency agile radar signals that are separated in frequency by an amount exceeding the coherence bandwidth will experience nearly independent fading. In this work it is assumed that the channel coherence bandwidth is sufficiently large compared with the radar pulse bandwidth so that no time-domain distortion of the received pulse occurs.

For a K^{-4} in situ power spectrum of three-dimensional ionization irregularities and one-way signal propagation path geometry with the radar and target on opposite sides of a scattering layer, the coherence bandwidth is given by

$$f_{coh} = \frac{\pi c(z_t + z_r)L_0}{r_e^2 \lambda^4 \ln(L_0/l_i) z_t z_r L \overline{\Delta N_e^2}} \,. \tag{8}$$

In this expression, c is the velocity of light in vacuum, z_t is the distance from the transmitter to the center of the ionized layer, z_r is the distance from the target to the center of the ionized layer, and $z_t + z_r$ is the total one-way propagation distance. The relationship between one- and two-way propagation paths is discussed in *Knepp*, [1985]. To obtain the appropriate description of a two-way monostatic radar propagation geometry, reduce the values of τ_0 and f_{coh} on the one-way path by a factor of $\sqrt{2}$.

In general the signal power fluctuation due to variations caused by the propagation channel, S, exhibits correlation over both time and frequency as discussed above. However, in this work only the burst-to-burst correlation is of interest. Therefore, the resulting correlation function may be modeled as a frequency coherence function given by

$$C_{SS}(f_d) = \langle S(f)S(f + f_d)\rangle - \langle S\rangle^2 \tag{9}$$

where it is assumed that S is a stationary process over the frequency range of interest.

Consideration of channel coherence is important for the assessment of the effectiveness of burst combining using a frequency agile radar in a fading channel. If the separation of burst transmission frequencies is great enough to insure that $S(f)$ is uncorrelated, then radar performance will be greatly enhanced through burst combining. However, if the received power shows correlation from burst to burst, then it is important to account for C_{SS} in the calculation of detection probability.

SECTION 3

RADAR SYSTEM CHARACTERISTICS

In this report it is assumed that an SBR is required to operate through a disturbed ionospheric channel to detect and track targets near the earth's surface. Thus, relative to a ground based radar with similar functions, an SBR has several limitations. First, targets are detected and tracked at very long ranges. Second, available onboard transmitter power is relatively low. Third, because of the large target ranges involved, large areas of the earth's surface are illuminated with resultant large clutter returns, even with a very narrow antenna beamwidth.

The first two points imply low received signal-to-noise ratio per pulse and therefore require long integration times. However, the cross section of a moving target remains constant or coherent for only a few tens of milliseconds because of target motion and resulting constructive and destructive interference between many scattering centers. Hence, during a radar look, the total energy transmitted at a target is divided into a number of bursts. Each burst consists of some number, n, of pulses which are coherently integrated. This group of pulses will be referred to as a burst. Multiple bursts may be transmitted to form a look, with each burst transmitted at a different frequency in the case of a frequency hopping radar. The detected amplitude of all the bursts which form the total radar target look are then noncoherently combined in a postdetection integration process. The resulting signal power is then compared to a threshold level to decide whether or not a target has been detected during the radar look.

One reason for choosing a waveform consisting of many coherently related pulses is that the radar transmitter may be power limited and unable to generate sufficient energy in a single pulse. Thus many pulses with low power are coherently transmitted, then coherently integrated on reception to achieve high signal-to-noise ratio. A second advantage in using a coherent pulsed radar waveform is that doppler processing techniques may be applied to the pulses comprising a single burst to achieve clutter suppression.

The use of frequency hopping can produce independent samples of the target cross section from burst to burst. Depending on the target geometry and motion relative to the radar, the target cross section from burst to burst may also be independent. In either case a Swerling II cross section model applies. Since a nonfluctuating

target serves as a convenient reference for computation and is also of interest for many types of defense systems, results are also given for this target model.

When the time duration of a burst is short enough so that the received signal power remains essentially constant within a burst, then the fading is referred to as slow fading. The slow fading assumption will be assumed to apply for all cases considered in this report.

Two types of radar detection techniques are considered here, namely double threshold detection and noncoherent integration. In both techniques the first stage is quadrature detection of the radar return from a transmitted burst. The quadrature detector output is a measure of received power. For the M out of N detection scheme, N bursts are transmitted to form a look. If the power received from M or more bursts exceeds a predetermined threshold, then a detection is declared. In the case of noncoherent integration, the power measured from each burst in a look is summed and if the resultant sum exceeds a threshold, then a detection is declared.

A phased-array radar system having sufficient beam pointing flexibility might utilize a modified M out of N detection scheme. For example, if a hit is declared on the first M bursts, the rest need not be transmitted. For a radar that must detect multiple targets, additional bursts may be transmitted to a specific location upon a threshold crossing of the return from the first burst.

SECTION 4

PROBABILITY OF DETECTION

The goal of this section is to develop methods to obtain the probability of detection for a radar operating in the presence of scintillation. Mathematical expressions, which are readily evaluated using numerical methods, are found for the detection probability when constraints are placed on the burst correlation function of the random process S_i - the fractional change in signal power in burst i due to variations caused by the propagation channel. For the remaining cases, the detection probability is calculated via Monte Carlo simulation methods. The simulation method presented here is general enough to include any coherence function for S.

Expressions that may be readily evaluated numerically are developed for the following cases: M out of N detection of both constant and Swerling II targets when the received power S is assumed independent from burst to burst, M out of N for both constant and Swerling II targets when S is assumed identical for each burst in a look, and noncoherent integration of bursts for a Swerling II target when S is assumed identical for each burst in a look. In all cases S is assumed to follow a Nakagami-m amplitude distribution.

Monte Carlo methods developed here may be used to determine the probability of detection for both M out of N detection and noncoherent integration for a Swerling II target. The received signal power fluctuation due to propagation for each burst, S_i, follows an arbitrary correlation function and a Nakagami-m amplitude distribution.

4.1 RECEIVER MODEL.

Under slow fading conditions let the signal amplitude and phase during a received radar burst be constant so that the in-phase and quadrature voltage components are given by the expressions

$$i = a\cos\phi + n_i \tag{10}$$

$$q = a\sin\phi + n_q \tag{11}$$

where i is the voltage (signal plus noise) of a single burst in the in-phase channel and q is the voltage of a single burst in the quadrature channel. The total average signal power is $\langle i^2 \rangle + \langle q^2 \rangle = S_r$. The noise is assumed to be additive white Gaussian noise with probability density function

$$p(n_i) = \frac{1}{\sqrt{2\pi}\sigma_N} \exp\left\{-\frac{n_i^2}{2\sigma_N^2}\right\} \tag{12}$$

with a similar expression for $p(n_q)$. The total noise power per burst is

$$\langle n_i^2 \rangle + \langle n_q^2 \rangle = 2\sigma_N^2 \tag{13}$$

so that the signal-to-noise ratio per burst is $S_r/2\sigma_N^2$. Now the output voltage from a quadrature detector giving $w = (i^2 + q^2)^{1/2}$ has the well-known Rician probability density function conditioned on S_r

$$p(w|S_r) = \frac{w}{\sigma_N^2} \exp\left\{\frac{-(w^2 + S_r)}{2\sigma_N^2}\right\} I_0\left(w\sqrt{S_r}/\sigma_N^2\right) \tag{14}$$

where I_0 is the modified Bessel function. The above density function may also be conditioned jointly on S and σ through the use of Equation 1. For a Swerling II target, the probability density function of the target cross section is given by Equation 2. Now since S and σ are independent variables, a conditional density with respect to S alone is obtained via

$$p\,(w|S) = \int_0^\infty p\,(\sigma)\, p\,(w|S_r = [S_0 S\sigma/\langle\sigma\rangle])\, d\sigma \tag{15}$$

where $S_r = S_0 S\sigma/\langle\sigma\rangle$. The integral expression in Equation 15 easily reduces to the conditional density for w.

$$p\,(w|S) = \frac{w}{\sigma_N^2\,(1 + S_0 S/2\sigma_N^2)} \exp\left\{\frac{-w^2}{2\sigma_N^2\,(1 + S_0 S/2\sigma_N^2)}\right\}, \text{ Swerling II target} \tag{16}$$

4.2 NONFLUCTUATING TARGET.

For a nonfluctuating target the probability density function of the target cross section can be represented by the Dirac delta function $\delta(\sigma - S_0)$. In this case the integration in Equation 15 gives

$$p(w|S) = \frac{w}{\sigma_N^2} \exp\left\{\frac{-(w^2 + S_0 S)}{2\sigma_N^2}\right\} I_0\left(w\sqrt{S_0 S}/\sigma_N^2\right), \text{ constant target} \qquad (17)$$

Note that the mean received power for both the Swerling II and the constant target is $S_0 S + 2\sigma_N^2$ as it should be.

4.3 SINGLE BURST DETECTION.

The quadrature detector output is compared to a preset threshold at the end of a burst interval, and a "hit" or a "miss" is declared. The threshold is set on the basis of the noise alone so that the probability of false alarm is small The probability of a false alarm for detection of a single burst is given by

$$p_{fa} = \int_{th}^{\infty} p(w|S = 0)\, dw \qquad (18)$$

The quantity p_{fa} is simply the single-burst probability that the noise amplitude alone exceeds the threshold. The above equation is integrated to obtain the familiar result

$$th = \sqrt{-2\sigma_N^2 \ln(p_{fa})} \qquad (19)$$

Thus the threshold amplitude is expressed as a function of the RMS noise amplitude and the desired probability of false alarm for a single burst. The threshold is the same for all channel and target models, since the noise is independent of target and channel statistics.

Equations 15 and 19 may be used to find the single-burst probability of detection as a function of S, the fractional change in signal amplitude due to scintillation.

$$
\begin{aligned}
p_d(S) &= \int_{th}^{\infty} p\,(w|S)\,dw \\
&= p_{fa}^{(1+S\langle SNR\rangle)^{-1}}, \text{ Swerling II target or} \\
&= Q\left(\sqrt{-2\ln\left(p_{fa}\right)}, \sqrt{2S\langle SNR\rangle}\right), \text{ constant target}
\end{aligned} \tag{20}
$$

where $\langle SNR\rangle = S_0/2\sigma_N^2$ is the average signal-to-noise ratio at the amplitude detector output and Q is the Marcum-Q function [*Marcum*, 1948]. When $S = 1$, Equation 20 is the familiar formula for detection probability of a Swerling II target.

4.4 M OUT OF N DETECTION.

In the case of M out of N or double threshold detection, it is straightforward to obtain simple analytic expressions for the overall probability of detection in terms of the probability of detection per burst, provided that the radar returns from each burst are independent.

Now assume that the probability of detection per burst is given by p_d. To find the overall probability of detection, P_D, let $p_b(i,j)$ be the probability of obtaining exactly i detections in j bursts. Then the probability of obtaining M or more detections out of N bursts is the sum

$$
\begin{aligned}
p\,(M,N) &= p_b\,(M,N) + p_b\,(M+1,N) + \cdots + p_b\,(N,N) \\
&= \sum_{k=M}^{N} P_b(k,N)
\end{aligned} \tag{21}
$$

but since p_b is given by the binomial distribution [*Feller*, 1957],

$$
P_b(i,j) = \binom{j}{i} p_d^i (1-p_d)^{j-i} \tag{22}
$$

then it is easy to obtain the probability of detection for the M out of N process,

$$
P_D = \sum_{k=M}^{N} \binom{N}{k} (p_d)^k (1-p_d)^{(N-k)} \tag{23}
$$

In the absence of a target, the overall probability of false alarm for double threshold detection is given by a similar expression

$$P_{FA} = \sum_{k=M}^{N} \binom{N}{k} (p_{fa})^k (1 - p_{fa})^{(N-k)} \tag{24}$$

where p_{fa} is the single-burst false alarm probability.

4.5 INDEPENDENT BURSTS.

Now consider the case that the contribution to the received signal due to channel fluctuations is independent from burst to burst, either due to temporal or frequency offsets between bursts. Here the probability of detection for a single burst is obtained by averaging $p_d(S)$, given by Equation 20, over the distribution of channel fluctuations $p_2(S)$.

$$p_d = \int_0^\infty p_d(S) p_2(S) dS \tag{25}$$

where $p_2(S)$ is given by Equation 5.

4.6 CONSTANT PROPAGATION CHANNEL.

Now consider the case that the contribution to the received signal due to the disturbed channel is constant over all the bursts that comprise a look. In this case the probability of detection during fading is computed by averaging the probability of detection for constant propagation conditions over the appropriate distribution function describing the propagation channel fluctuations. In this case the overall detection probability may be written as

$$P_D = \int_0^\infty \left[\sum_{k=M}^{N} \binom{N}{k} (p_d(S))^k (1 - p_d(S))^{N-k} \right] p_2(S) dS \tag{26}$$

where $p_d(S)$ is given by Equation 20.

4.7 NONCOHERENT INTEGRATION - CONSTANT PROPAGATION CHANNEL.

For a Swerling II target and a constant propagation channel, *Dana and Knepp* [1986] have developed a general formulation for the case of noncoherent integration that may be applied to the case of Nakagami-m statistics. The detection probability is evaluated using the expression

$$P_D = \int_0^\infty P_D(S) p_2(S) dS \tag{27}$$

where $p_2(S)$ is given by Equation 5 and where

$$P_D(S) = \frac{\Gamma\left\{M, th/\left[\sigma_N^2 \left(1 + S(SNR)\right)\right]\right\}}{\Gamma(M)} \tag{28}$$

$$\Gamma(a,t) = \int_t^\infty t^{a-1} e^{-t} dt \tag{29}$$

and the threshold is set using

$$P_{FA} = \Gamma\left(M, th/\sigma_N^2\right) / \Gamma\left(M\right) \tag{30}$$

$\Gamma(m)$ is the usual gamma function of a single argument and $\Gamma(a,t)$ is an incomplete gamma function. Equation 29 is easily inverted numerically to give th/σ_N^2 as a function of the probability of false alarm and the number of bursts M.

4.8 NUMERICAL METHODS.

It is straightforward to numerically evaluate the foregoing integral expressions for probability of detection. For the case of M out of N detection, using specified values of M, N and the overall probability of false alarm, P_{FA}, the first step is the numerical inversion of Equation 24 to obtain the single-burst probability of false alarm, p_{fa}. If desired, the threshold is then obtained using Equation 19. The quantity p_{fa} is used in Equation 20 to obtain $p_d(S)$ and the integrals of Equations 25 and 26 are

performed as desired. This entire process is repeated as often as desired for different values of signal-to-noise ratio and scintillation index.

A similar procedure is used for the case of the noncoherent combining of bursts from a Swerling II target in a constant propagation channel.

4.9 GENERAL CORRELATION OF BURST RETURNS.

In the general case of a disturbed propagation channel, the radar returns from the bursts that comprise a look will exhibit some degree of correlation in time and frequency as discussed earlier. In this case, the use of numerical integration techniques becomes prohibitive because the probability of detection is expressed as multivariate integrals. Therefore, Monte Carlo simulation techniques must be used to obtain the probability of detection for the case that burst-to-burst correlation is described by a general correlation function. The techniques described below are valid for general correlation functions of any form. However, in the examples to be presented, a simple Gaussian function is used. This simple one-parameter distribution is quite useful since a Gaussian function is often used to fit more complicated distributions.

The simulation is carried out by generating random samples of the received signal power, S_r, for each burst within a look. The resulting samples may be processed directly using either double-threshold detection or noncoherent integration. After a sufficient number of looks are processed, an estimate is obtained of the detection probability at a given SNR and probability of false alarm.

In order to have a valid representation of the fading channel, it is required that the statistics of received power follow the Nakagami-m distribution. Fortunately, as noted previously, the χ^2 number of degrees of freedom is related to the Nakagami-m parameter by the expression $m = n/2$, $n = 1, 2, 3 \cdots$. A useful range of values of S_4 may be obtained using the available half-integer values of m.

A χ^2 variate with n degrees of freedom may easily be generated from the expression

$$S = v_1^2 + v_2^2 + \cdots + v_n^2 \tag{31}$$

where the v_i are independent, zero mean Gaussian variates with variance σ_v^2 selected so that the mean value of S is unity.

It is also required that all values of power S for bursts in a single look be related according to the arbitrary correlation function C_{SS}. Write S as a function of the index of the burst, i, where there are N bursts per look and $i = 0, 1, \cdots, N-1$. Therefore, it is required that

$$\begin{aligned} C_{SS}(j) &= \langle S(i)S((i+j),\ \text{mod N})\rangle - \langle S\rangle^2 \\ j &= -(N-1), \cdots, (N-1) \end{aligned} \tag{32}$$

where the notation "mod" refers to the modulo remainder function defined by $(a,\ \text{mod N}) = r$ where $a = r + nN$ and n is any integer or zero.

Expanding Equation 31 for all bursts in a look gives a set of equations

$$\begin{array}{lcccccccc} S(1) & = & v_1^2(1) & + & v_2^2(1) & + & v_3^2(1) & +\cdots+ & v_n^2(1) \\ S(2) & = & v_1^2(2) & + & v_2^2(2) & + & v_3^2(2) & +\cdots+ & v_n^2(2) \\ \vdots & & \vdots & & \vdots & & \vdots & & \vdots \\ S(N) & = & v_1^2(N) & + & v_2^2(N) & + & v_3^2(N) & +\cdots+ & v_n^2(N) \end{array} \tag{33}$$

Equation 33 may be satisfied if

$$C_{SS}(j) = 2nC_{vv}^2(j) \tag{34}$$

where

$$C_{vv}(j) = \langle v_k(i)v_k((i+j),\ \text{mod N})\rangle;\ \text{any k, any i} \tag{35}$$

The above assertion is easily proven using the relation [*Papoulis*, 1984]

$$\langle x^2y^2\rangle = \langle x^2\rangle\langle y^2\rangle + 2\langle xy\rangle^2 \tag{36}$$

where x and y are jointly normal with zero mean.

It is, therefore, necessary to generate n gaussian vectors, each of length N, that satisfy Equation 34 that are to be used in Equation 33. An efficient and flexible method for generating a vector of jointly normal variates is presented in *Hurst and Knop* [1972].

SECTION 5

RESULTS

In this section quantitative results are given for probability of detection for a wide range of scintillation conditions ranging from weak to strong scattering and for various amounts of decorrelation between bursts in a look. It is shown that both double threshold detection and noncoherent combining of bursts offer a degree of mitigation against the effects of scintillation when there is some diversity gain available through decorrelation of bursts in a look. Although the probability of false alarm is arbitrary in our formulation and is an input variable to the simulations, all results to be presented assume that the detection threshold is set so that the false alarm rate per look is 10^{-6}.

Figures 7 and 8 illustrate the effects of various levels of fading on a system employing a single burst for detection of a constant cross section target and a Swerling II target, respectively. The figures show probability of detection as a function of the mean signal-to-noise ratio per burst. It is useful to compare these figures at various values of detection probability. Generally a single-burst probability of detection of about 0.5 or greater is needed for successful tracking. For example, from Figure 7 at a value of probability of detection of 0.7, the loss in detection sensitivity relative to undisturbed conditions is about 3.5 dB at a value of S_4 of 0.5 and about 11 dB at a value of S_4 of 1.0. Figure 8 shows similar losses in sensitivity relative to undisturbed conditions for a Swerling II target model. With the exception of very low SNR, radar performance is better for the constant target cross section model relative to the Swerling II model due to the decreased variability in received signal power.

In Figures 9-27 the effect of M out of N burst combining is investigated for various values of M and N. In these figures the abscissa is the signal-to-noise ratio per look defined as N times the signal-to-noise ratio per burst. Thus the curves are plotted so that various combinations of M and N may be compared on the basis of an equal amount of transmitted energy per look, on the assumption that all N bursts are transmitted on each look.

Figures 9-10 give radar detection performance for the two target models for the case of an undisturbed propagation channel. Figure 9 shows the effect of using multiple bursts per look against a constant cross section target with no propagation channel fading. The optimum number of bursts per look is one and there is no advantage from burst combining. When the target statistics obey the Swerling II

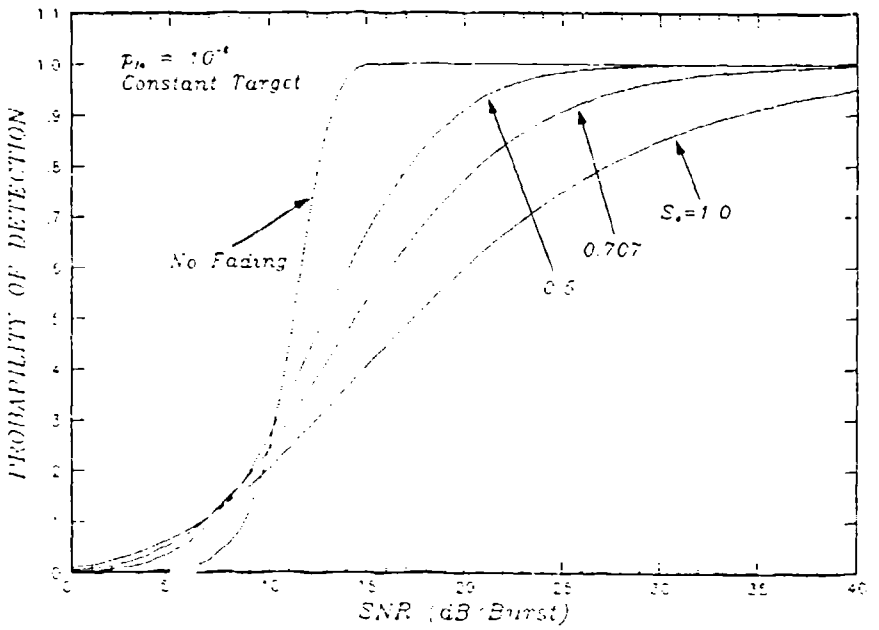

Figure 7. Probability of detecting a constant target with a single burst for various scintillation levels.

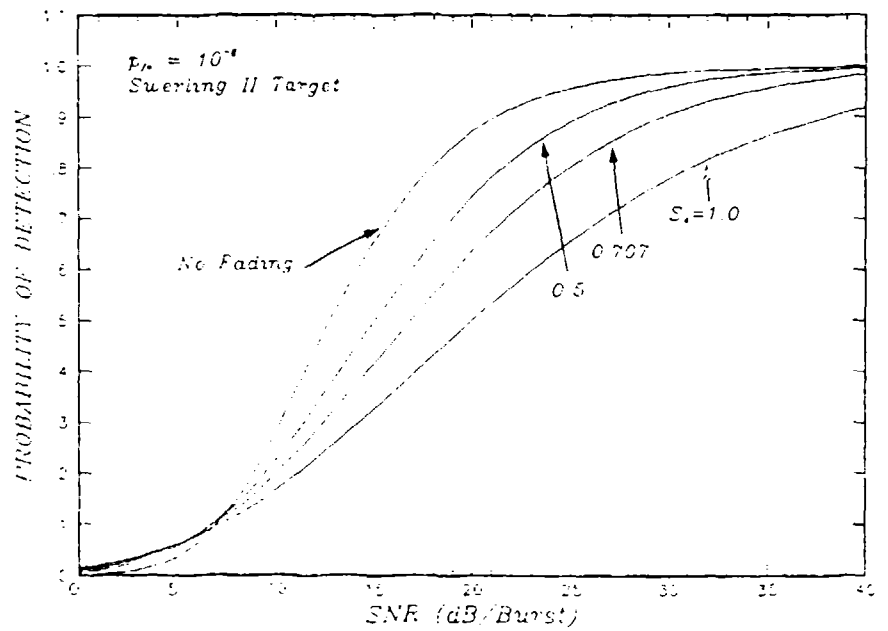

Figure 8. Probability of detecting a Swerling II target with a single burst for various scintillation levels.

model, however, the received signal power varies independently from burst to burst, and diversity combining is effective as shown in Figure 10. At a value of probability of detection of 0.8, 1 out of 2 burst combining improves detection sensitivity about 1 dB relative to no combining (i.e., 1 out of 1). The results presented in Figures 9-10 are well known. However, these figures are included to allow the reader to visually compare the results for detection in a benign propagation environment with the results to be presented for a fading channel.

In Figures 11-18 quantitative results for probability of detection are given that show the effect of various levels of scintillation severity on double threshold detection for both target models of interest here. For these results, it is assumed that the signal contribution due to channel fading is independent from burst to burst within a look. This case of the propagation channel disturbance is referred to as Type II fading, not unlike a Swerling II target model.

Figures 11-12 show radar detection performance for the two target models for an S_4 value of 0.5 on the one-way propagation path. This value of S_4 is generally accepted as marking the transition from weak to strong scattering. Figure 11, for a constant target, shows that diversity combining does offer a slight advantage for 1 out of 2 combining for detection probabilities greater than 0.7. At lower detection probability or with the use of more than two bursts per look, diversity combining gives a loss in detection sensitivity. In the case of Swerling II target statistics, 1 out of N combining is seen to offer some improvement for all values of N shown (2,4,8) in Figure 12 when the detection probability is greater than 0.6. For example, at a probability of detection of 0.75, there is a gain of about 2 dB for the case of 1 out of 2, 4, or 8 relative to single-burst detection.

Figures 13-14 show detection performance for a value of S_4 of 0.707. From Figure 13, for a constant target, it is seen that there is a modest gain available for SNR values greater than about 13 dB per look, with the amount of gain depending on the number of bursts per look and on the SNR. At a probability of detection of 0.75 there is about 1.5 to 2.0 dB gain in detection sensitivity for multiple bursts per look.

From Figure 14, for a Swerling II target, a substantial gain in detection sensitivity is possible for values of probability of detection greater than 0.5. For example, at a probability of detection of 0.75 there is a 4.5 dB gain in using 1 out of 4 (or 8) rather than using a single burst.

Performance in worst-case scintillation, characterized by an S_4 scintillation index of 1.0 on the one-way propagation path, is considered in Figures 15-16. Figure 15

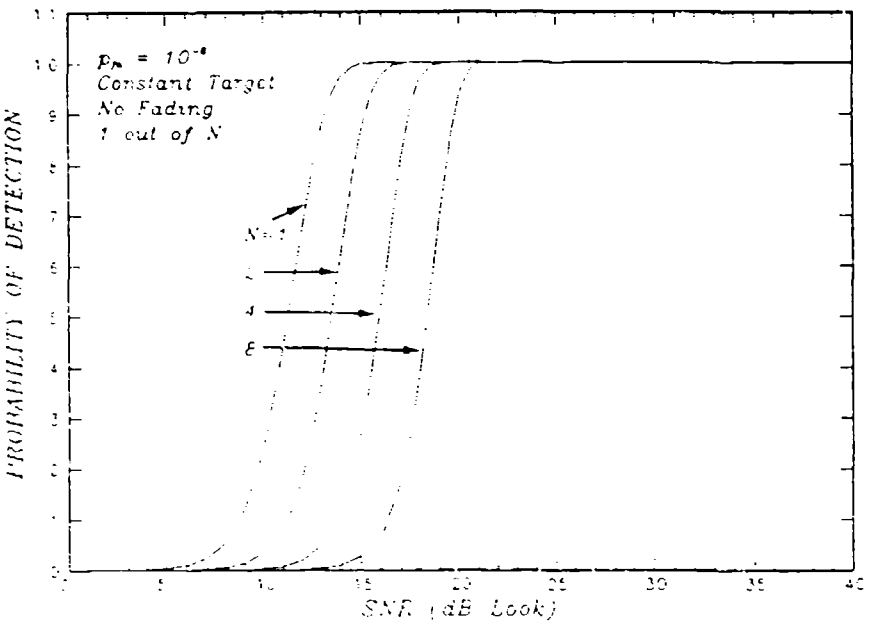

Figure 9. Probability of detecting a constant target with no channel fading using 1 out of *N* combining.

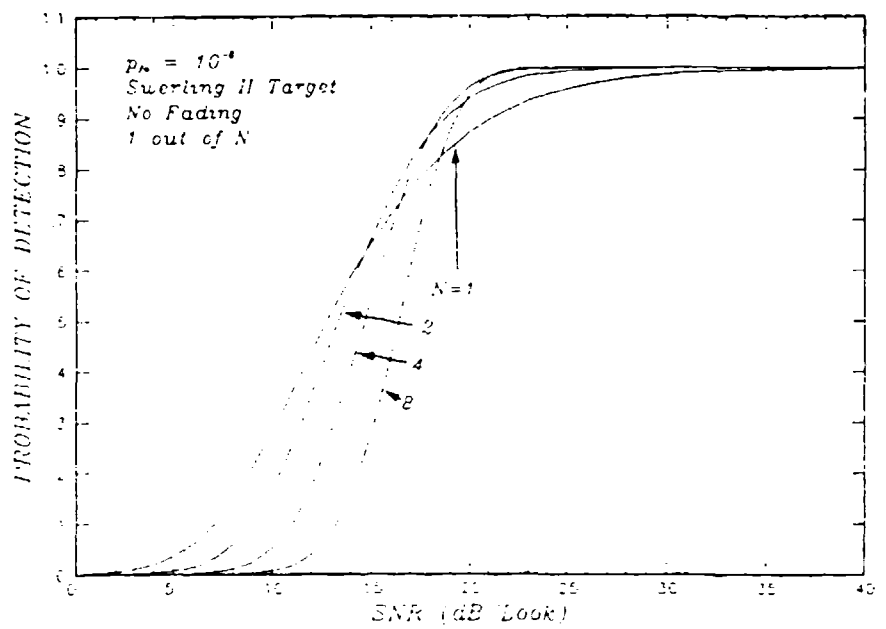

Figure 10. Probability of detecting a Swerling II target with no channel fading using 1 out of *N* combining.

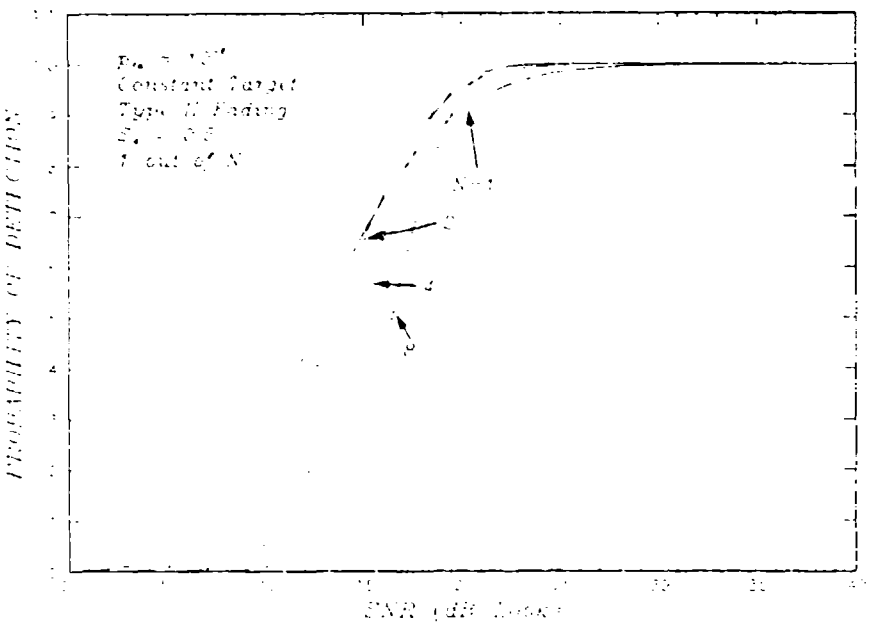

Figure 11. Probability of detecting a constant target with moderate (S_4 = 0.5) Type II fading using 1 out of N combining.

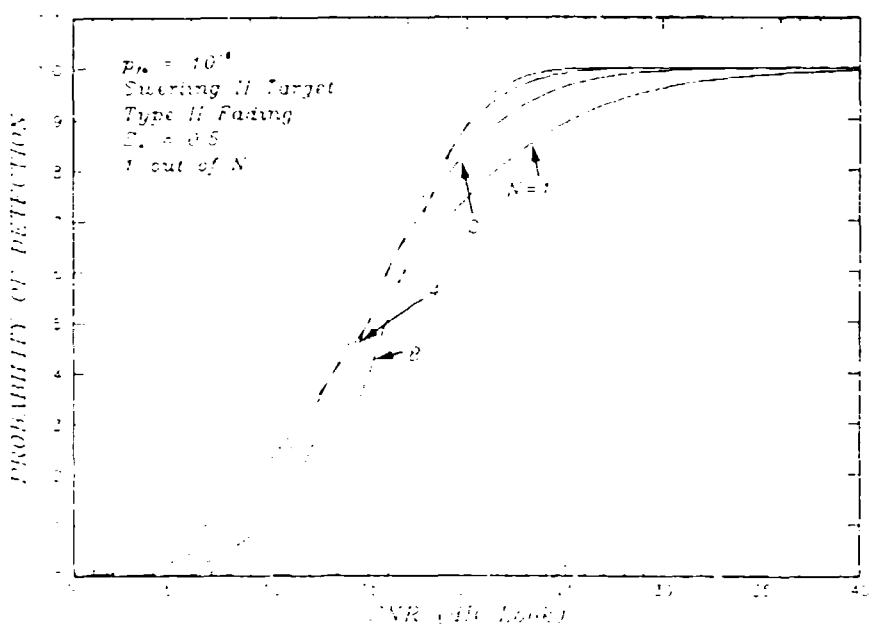

Figure 12. Probability of detecting a Swerling II target with moderate (S_4 = 0.5) Type II fading using 1 out of N combining.

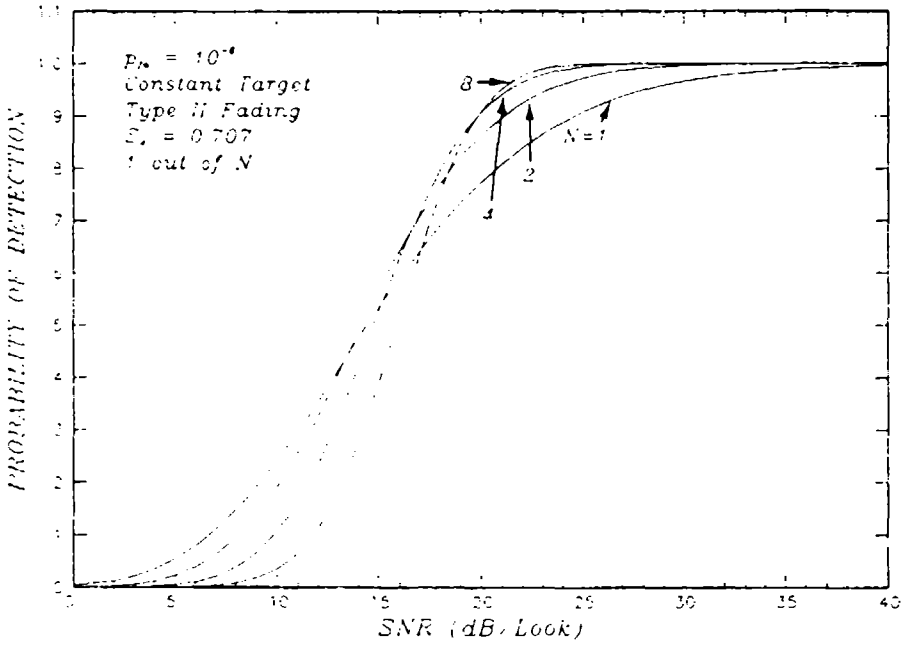

Figure 13. Probability of detecting a constant target with Type II fading and $S_4 = 0.707$ using 1 out of N combining.

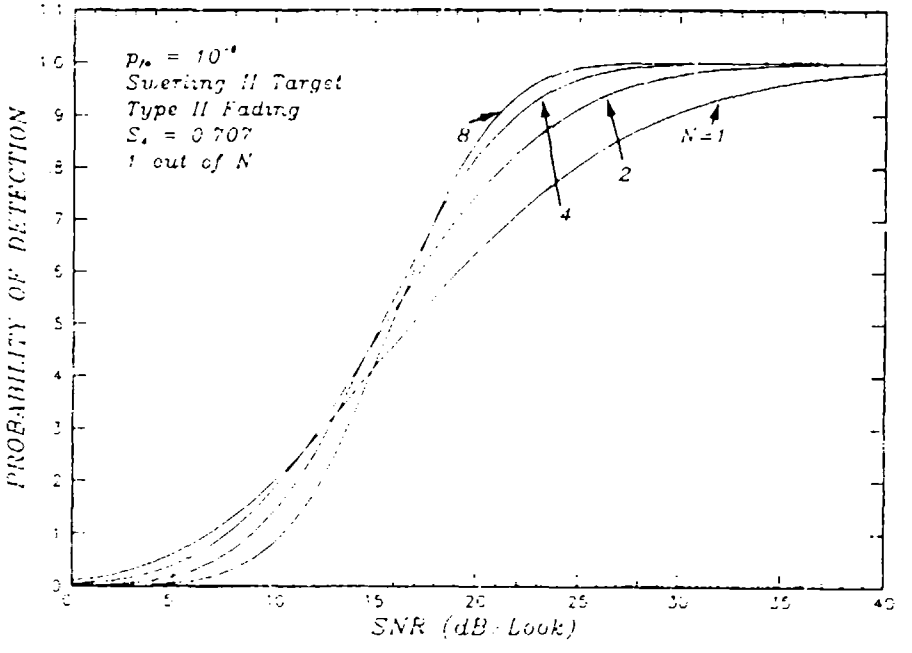

Figure 14. Probability of detecting a Swerling II target with Type II fading and $S_4 = 0.707$ using 1 out of N combining.

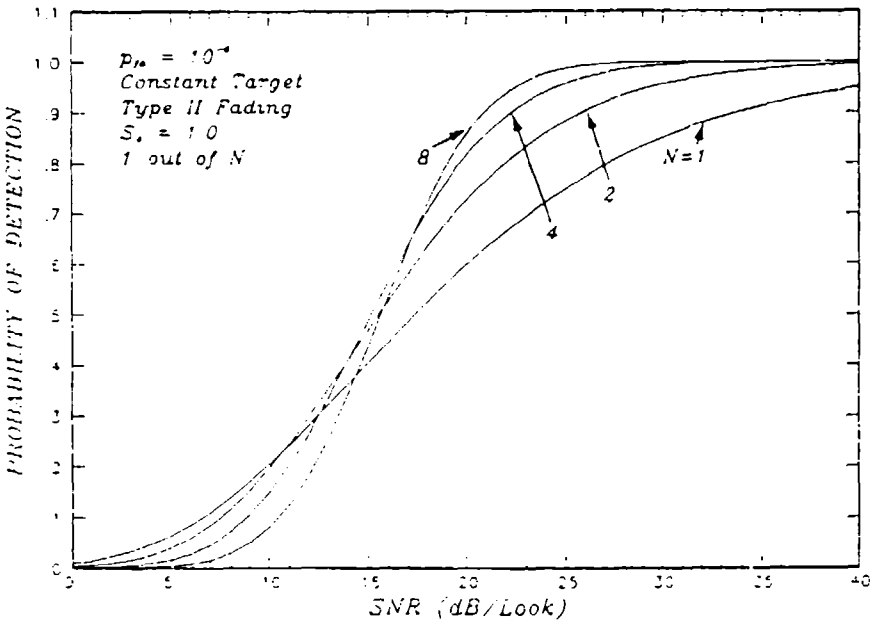

Figure 15. Probability of detecting a constant target with severe Type II fading ($S_4 = 1.0$) using 1 out of N combining.

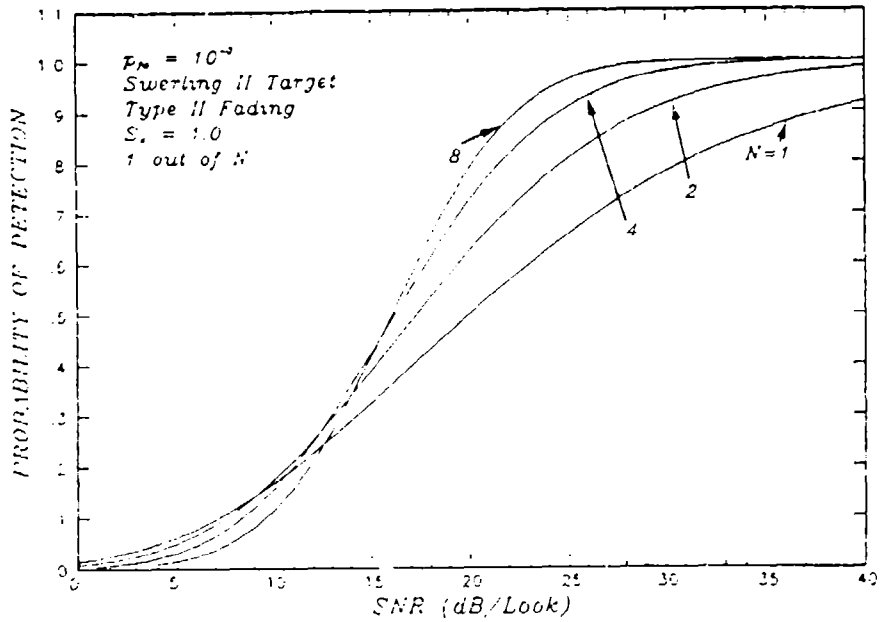

Figure 16. Probability of detecting a Swerling II target with severe Type II fading ($S_4 = 1.0$) using 1 out of N combining.

illustrates that, even for a constant target, diversity combining offers a performance improvement. An improvement of nearly 7 dB in detection sensitivity is available when the receiver operates at a detection probability of 0.75 using 1 out of 8 (or 4) detection. For the case of the Swerling II target model as shown in Figure 16, the use of 1 out of 8 (or 4) combining gives an improvement of about 4 dB at a detection probability of 0.5, and for a detection probability of 0.75 the improvement is 9.5 dB.

A comparison of Figures 11, 13 and 15 shows that, for a constant target and Type II fading, it is advantageous to use 1 out of N detection, provided that the value of S_4 is 0.707 or greater. For less severe scintillation, single-burst detection exhibits better performance. In the following, M out of N is considered further for values of M other than 1.

Figures 9-16 show the effect of variation of the number of bursts per look, N, for 1 out of N combining, on detection performance for constant and Swerling II targets. Various levels of Type II fading ranging from no fading to worst case fading ($S_4 = 1$) are considered. These figures illustrate that some protection against Type II fading is available using diversity combining. As an additional example illustrating the above point, compare Figures 17-18 with Figures 7-8, respectively. Figure 17 gives probability of detection using 1 out of 8 combining for a constant target model as a parametric function of the S_4 scintillation index. Results in Figure 7 are for an identical case except only a single burst is used. Note detection performance is not strongly affected by fading when 1 out of 8 combining is used. Also note that for a detection probability of 0.7, 1 out of 8 combining gives better performance in a strong fading environment than in a benign environment. Furthermore, performance is rather similar throughout the strong scattering regime. Of course, a large price is paid for using 1 out of 8 combining to detect a constant target in an undisturbed environment. Figures 8 and 18, for the case of a Swerling II target model, illustrate a similar situation. At a value of probability of detection of 0.7, a sensitivity loss of 1 dB is incurred when using 1 out of 8 combining as the propagation environment goes from no fading to worst case fading. However, the cost for using 1 out of 8 combining in an undisturbed environment is less than 2 dB relative to single burst detection at a detection probability of 0.7 for the Swerling II model.

5.1 TYPE I FADING.

The previous discussion has demonstrated the effectiveness of M out of N combining against Type II fading, where the effects of propagation channel scintillation are independent from burst to burst. If, however, the time and frequency scheduling

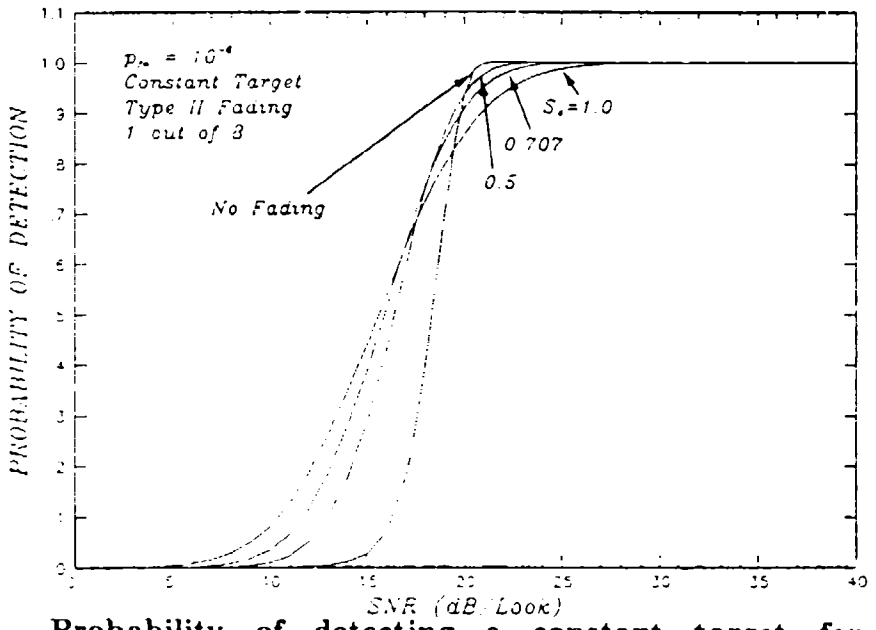

Figure 17. **Probability of detecting a constant target for various scintillation levels during Type II fading using 1 out of 8 combining.**

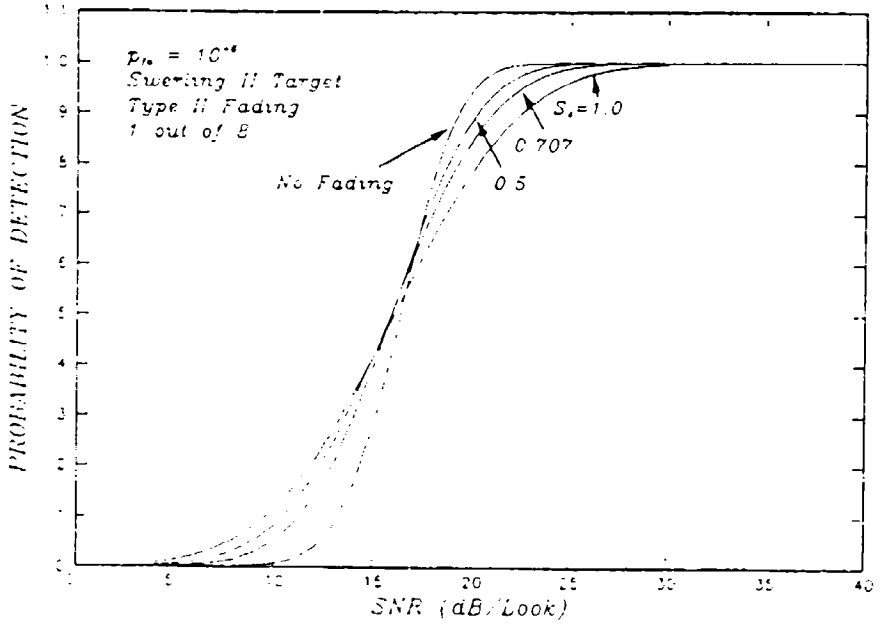

Figure 18. **Probability of detecting a Swerling II target for various scintillation levels during Type II fading using 1 out of 8 combining.**

of bursts is such that the effect of the propagation channel is identical from burst to burst (i.e., Type I fading), then diversity combining is no longer effective. Figures 19-20 show the effect of Type I fading on 1 and 2 out of 8 combining for values of S_4 of 0, 0.5, 0.707 and 1.0 for a constant and a Swerling II target, respectively. A comparison of these curves to those of Figures 7-8 which give single-burst detection performance shows that there is generally a loss suffered from combining in a Type I scintillation environment relative to using a single burst, for levels of scintillation severity where S_4 is greater than 0.5.

5.2 GENERAL BURST COHERENCE.

To investigate the effects of partial correlation on the performance of a frequency hopping radar, Monte Carlo simulations are performed using a Gaussian correlation function to describe the second-order statistics of the received power. The radar of interest is assumed to change frequency pseudo-randomly from burst to burst. In addition, the hopping sequence is assumed to be distributed uniformly over some hopping bandwidth, B_{hop}.

In general, the received power decorrelates over time and frequency as discussed in Section 2.4. This investigation will consider the case where the time separation between bursts is small enough relative to the decorrelation time to assume the received signal power does not decorrelate over time within a look. This assumption allows use of a coherence function that is a function of frequency only.

For this application a simple Gaussian correlation is chosen to represent the correlation of power from burst to burst.

$$C_{ss}(f) = \exp\left\{-(f/f_d)^2\right\} \tag{37}$$

where f_d is the decorrelation frequency. This simple Gaussian correlation function is chosen as the first application. By generating N uniform random burst frequencies over the hopping bandwidth, B_{hop}, and using Equation 37 to determine how the bursts are correlated, the methods of Section 4.9 may be used to generate realizations of the received signal power via Monte Carlo Simulation.

Detection performance results for 1 out of 8 combining for a Swerling II target are shown in Figures 21-23. The three figures give results for values of B_{hop}/f_d

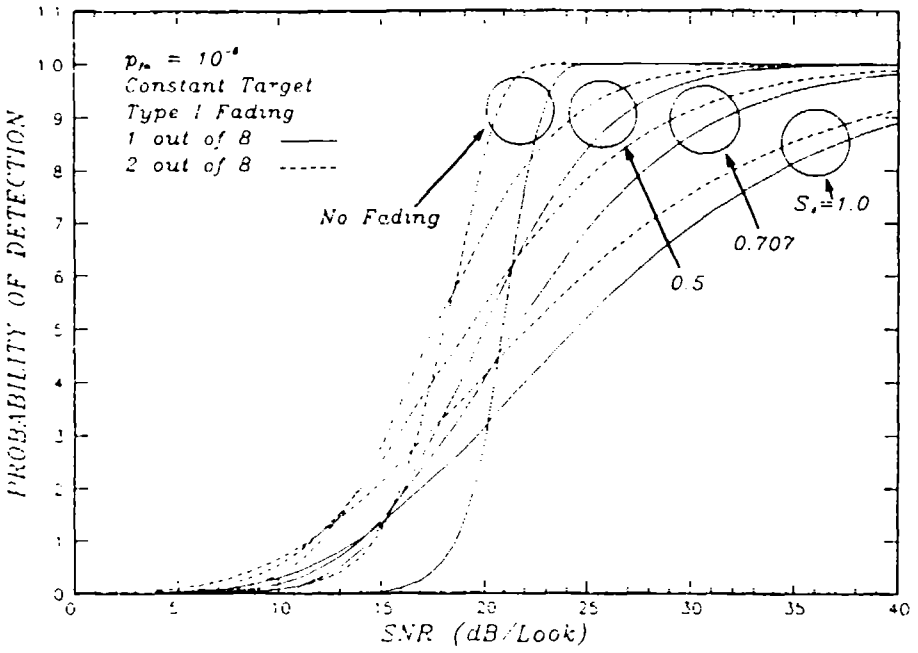

Figure 19. Probability of detecting a constant target for various scintillation levels during Type I fading using 1 and 2 out of 8 combining.

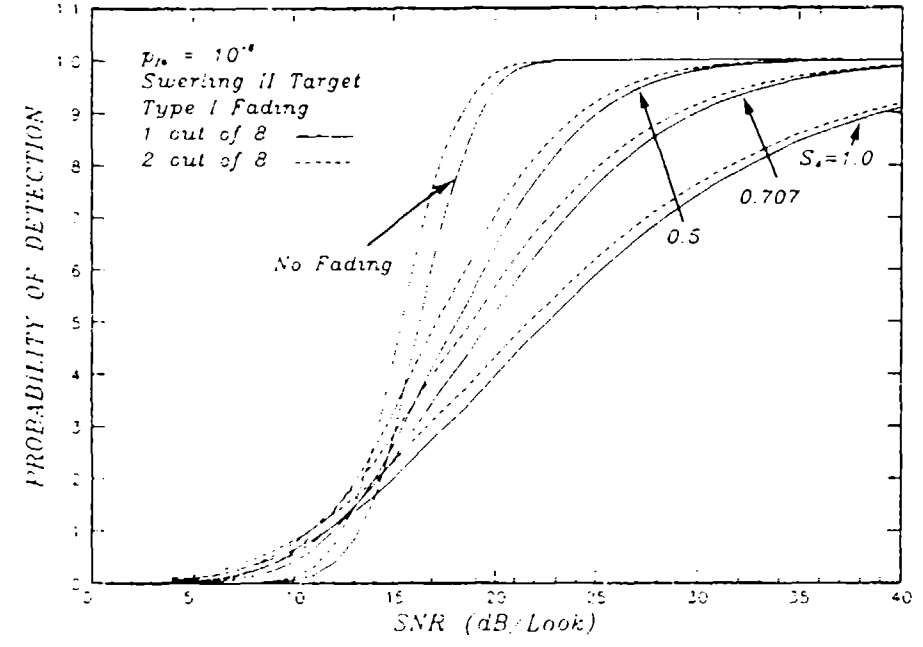

Figure 20. Probability of detecting a Swerling II target for various scintillation levels during Type I fading using 1 and 2 out of 8 combining.

of 10, 5, and 1. As B_{hop}/f_d increases, the expected correlation of bursts will also decrease. In general, performance will improve for larger values of B_{hop}/f_d.

Figure 21 gives the detection performance of 1 out of 8 combining for a Swerling II target for various values of scintillation index and $B_{hop}/f_d = 10$. Comparison of the curves for $S_4 = 1.0$ in Figure 21 and Figure 13 shows about a 1.5 dB loss in sensitivity at a probability of detection of 0.7 for $B_{hop}/f_d = 10$ when compared to the predicted performance assuming Type II fading. A similar comparison of Figure 22 with Figure 13 shows about a 3 dB loss in sensitivity when $B_{hop}/f_d = 5$.

As B_{hop}/f_d is lowered to 1, the preceding comparison, now made using Figure 23, indicates a loss in sensitivity of about 7 dB. More importantly, comparison of Figure 23 with Figure 3 (single burst detection) shows that for $S_4 = 1.0$ and a detection probability of 0.7, 1 out of 8 combining provides no diversity gain at this ratio of B_{hop}/f_d.

Additional results (not shown) indicate performance is essentially identical to that expected under the Type I fading assumption when $B_{hop}/f_d \leq 0.1$.

5.3 M OTHER THAN 1.

Figures 24-25 show the effect of variation in M on detection sensitivity for the case of an undisturbed propagation channel with a constant cross section target and a Swerling II target, respectively. For a constant target, detection performance is best using 4 (or 5) out of 8, with higher values of M yielding decreased detection sensitivity. Higher values of M are not shown in the figure for clarity. For a Swerling II target, 2 (or 3) out of 8 provide the best detection performance.

Figures 26-27 show probability of detection during Type II fading of different levels of severity using 2 out of 8 combining for a constant target and a Swerling II target, respectively. These figures can be directly compared to Figures 17-18 which give detection performance using 1 out of 8 combining. From the comparison it is seen that 1 out of 8 yields better detection performance than 2 out of 8 during strong scintillation conditions ($S_4 > 0.5$), but the reverse is true during weaker scattering ($S_4 < 0.5$). Note, however, this advantage is dependent on the assumption above of Type II fading, as may be seen by comparing Figures 21-23 for different amounts of burst-to-burst correlation.

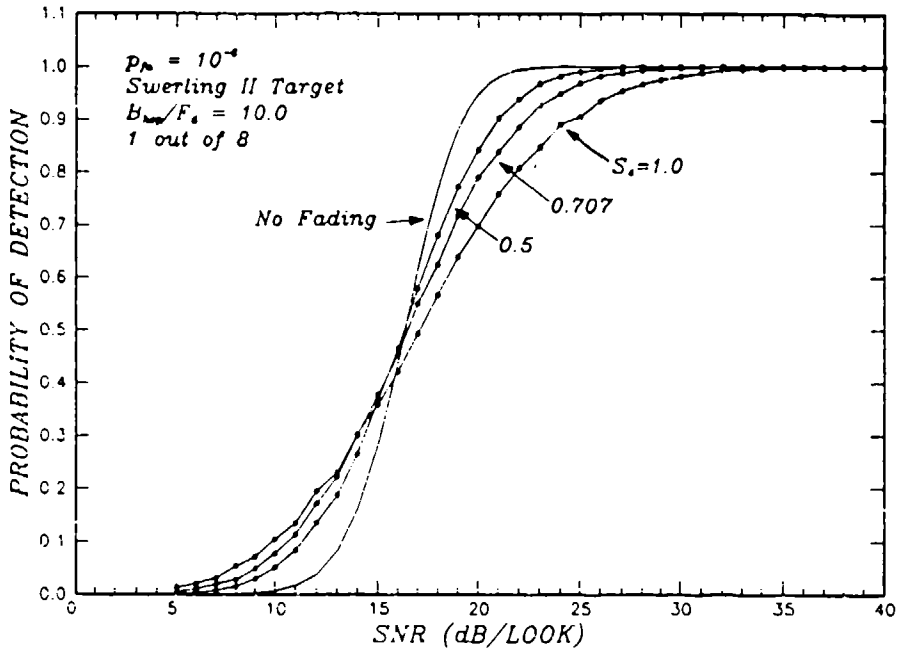

Figure 21. **Probability of detecting a Swerling II target using 1 out of 8 for various scintillation levels assuming Gaussian correlation of bursts, $B_{hop}/f_d = 10$.**

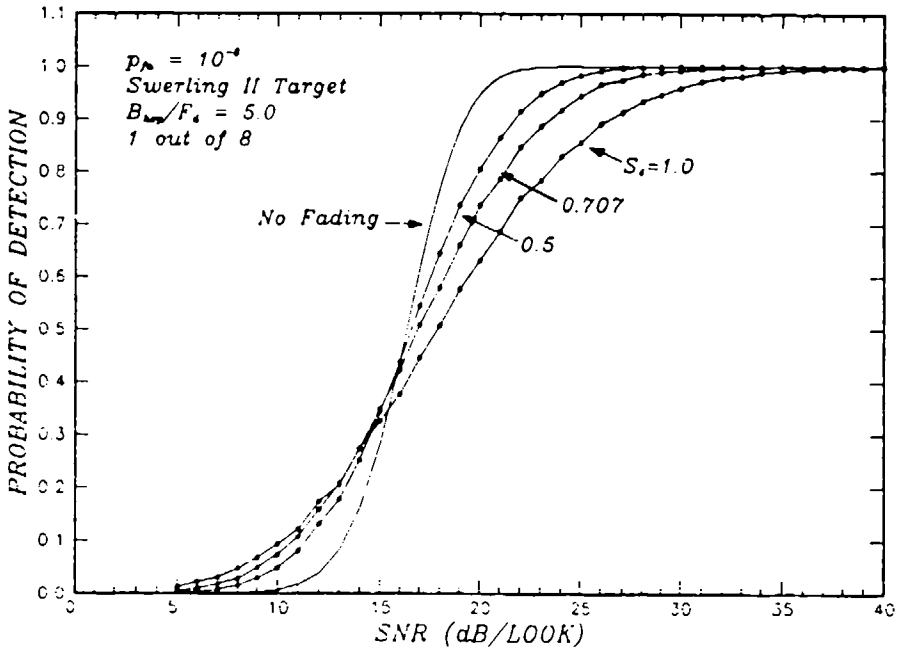

Figure 22. **Probability of detecting a Swerling II target using 1 out of 8 for various scintillation levels assuming Gaussian correlation of bursts, $B_{hop}/f_d = 5$.**

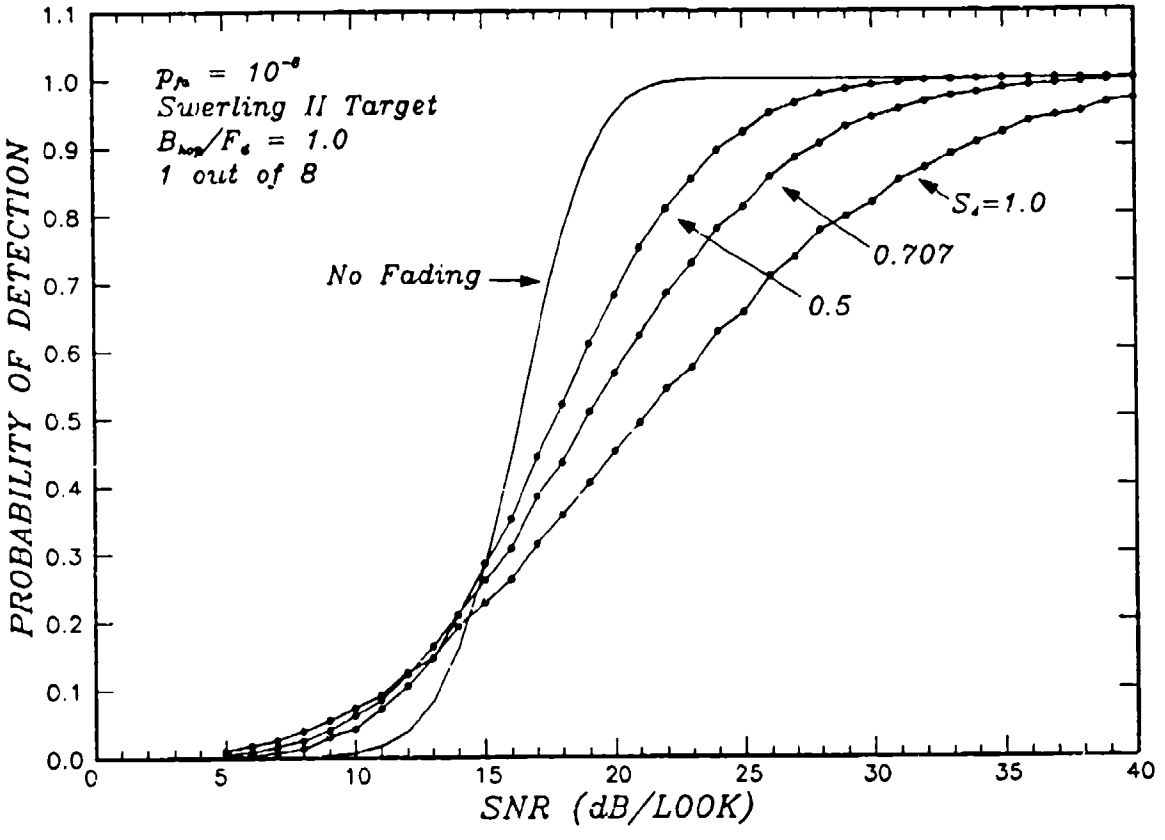

Figure 23. **Probability of detecting a Swerling II target using 1 out of 8 for various scintillation levels assuming Gaussian correlation of bursts, $B_{hop}/f_d = 1$.**

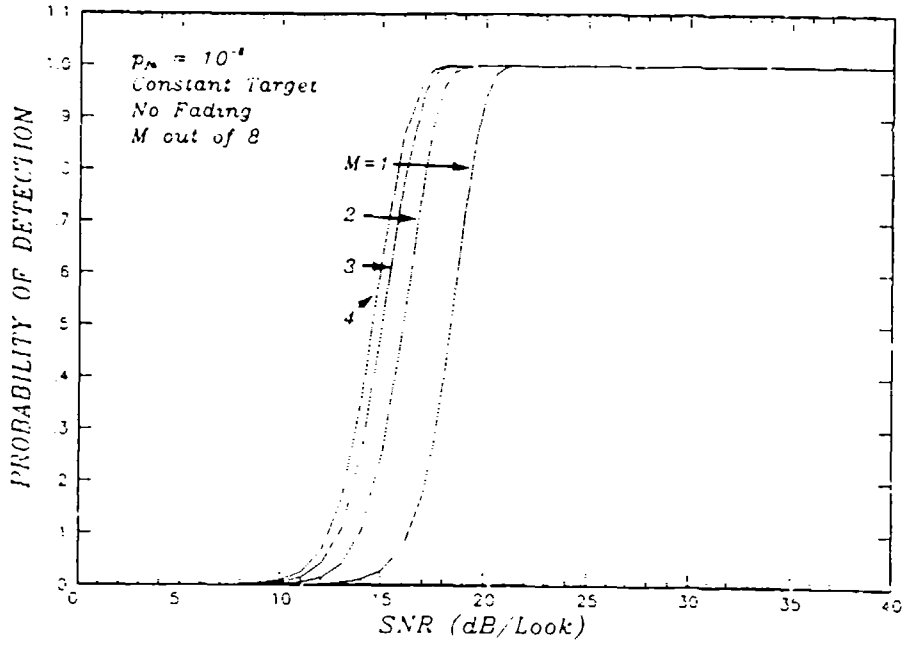

Figure 24. Probability of detecting a constant target with no fading using *M* out of 8 combining.

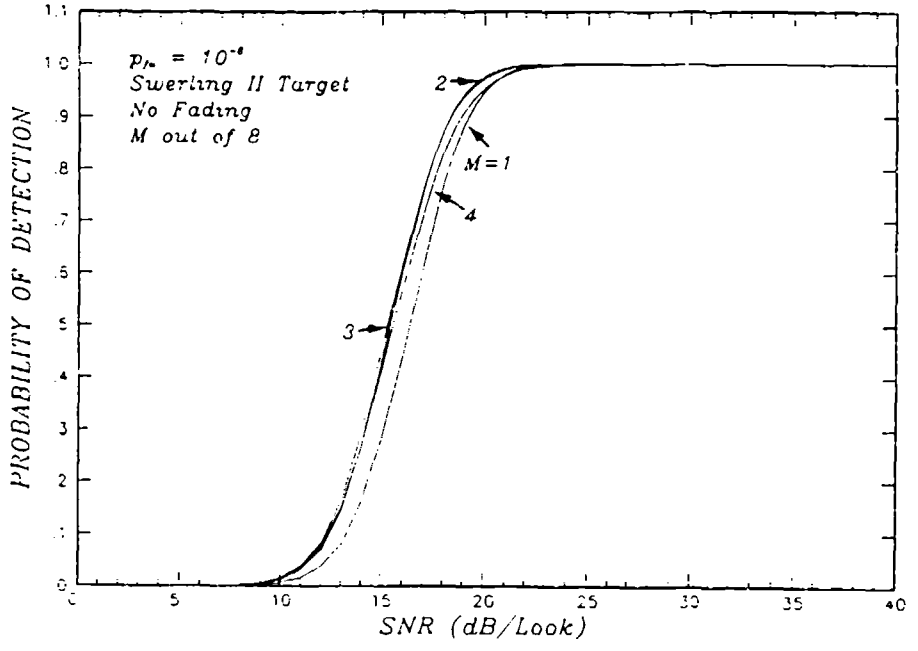

Figure 25. Probability of detecting a Swerling II target with no fading using *M* out of 8 combining.

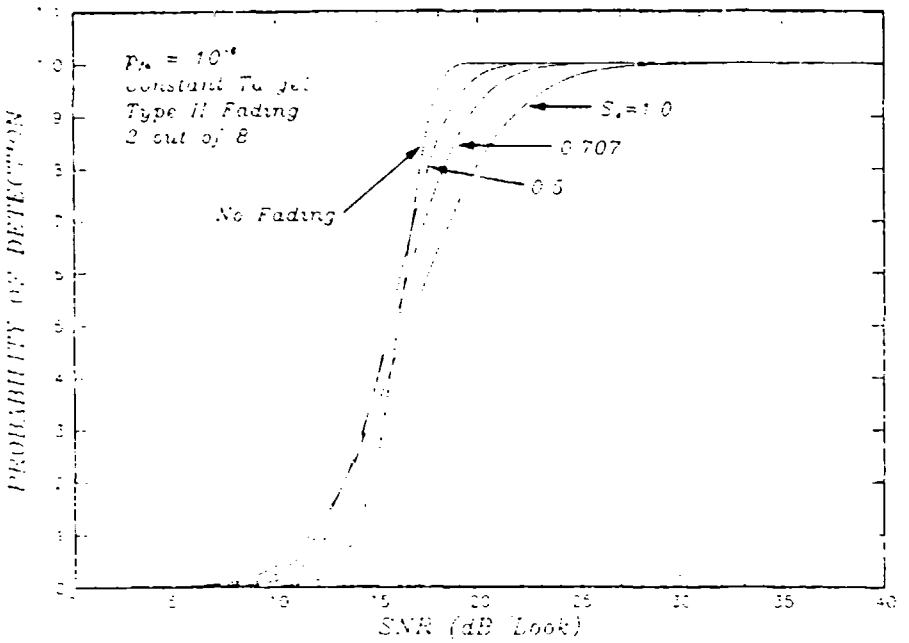

Figure 26. Probability of detecting a constant target during Type II fading using 2 out of 8 combining.

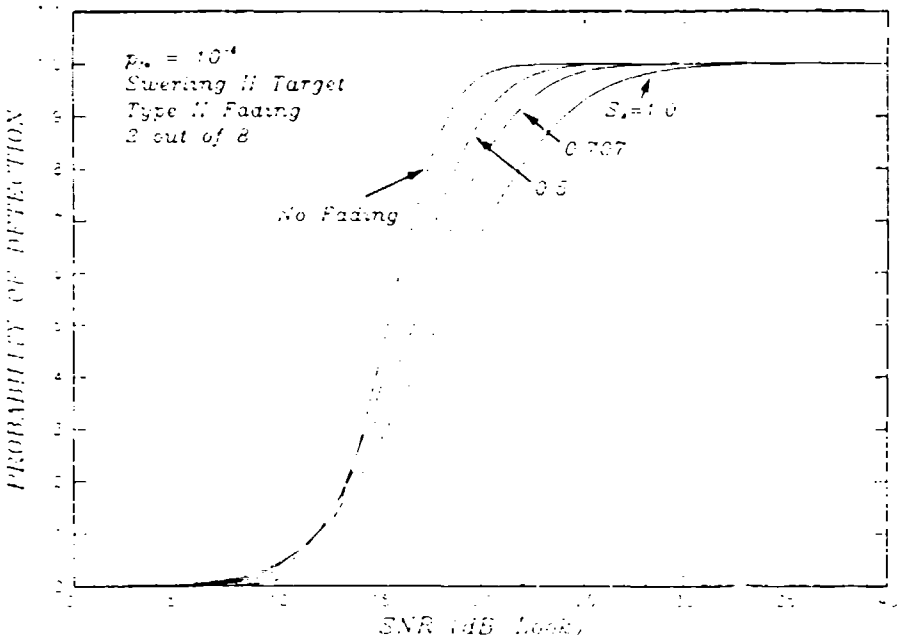

Figure 27. Probability of detecting a Swerling II target during Type II fading using 2 out of 8 combining.

5.1 NONCOHERENT INTEGRATION.

Results are presented in this section for detection using noncoherent integration of bursts for comparison with the previous results for double-threshold detection. Double threshold detection is sometimes referred to as binary integration since it can be considered a modification of noncoherent integration. The modification is that the output of the quadrature detector is A/D converted using 1 bit of resolution (threshold detection) prior to integration. Since, clearly, some information is lost when using such a coarse measure of the quadrature detector output, one can expect a penalty to be exacted in detection sensitivity for using double-threshold detection. Results in this section illustrate this loss in detection sensitivity for Swerling II targets.

Figure 28 shows the probability of detection for noncoherent integration for no fading and various values of N, the number of bursts per look. This figure can be compared with Figure 10 for double-threshold detection using 1 out of N. From Figure 28 it is seen that for noncoherent integration and a Swerling II target, the more bursts per look the better, provided that the signal-to-noise ratio is sufficiently high to maintain the probability of detection at about 0.5 or greater and thereby avoid the abrupt degradation in detection performance with decreasing SNR. On the other hand, from Figure 10, for double threshold detection using 1 out of N in an undisturbed propagation environment, only 1 out of 2 is generally useful.

Figures 29-33 give results for the probability of detecting a Swerling II target using noncoherent integration of 8 bursts per look under various conditions of scintillation severity and degrees of correlation of the bursts of a look. In all five figures, curves are shown for the case of no fading and for values of one-way S_4 of 0.5, 0.707, and 1.0. Figure 29, for Type II fading, may be compared directly with Figures 18 and 27 for double threshold combining using 1 or 2 out of 8. In the case of S_4 equal to or greater than 0.5, 1 out of 8 gives better performance than 2 out of 8. However, it is seen from a comparison of Figures 18 and 29 that noncoherent integration of 8 bursts enjoys an advantage of about 1.5 dB in comparison to double threshold detection using 8 bursts per look.

Figure 30, 31, and 32 show detection performance for the case of partially correlated bursts in a look with values of B_{hop}/f_d = 10, 5, and 1, respectively, and may be directly compared to Figures 21, 22, and 23. These comparisons indicate that noncoherent detection using 8 bursts per look enjoys an advantage of about 2 dB relative to double threshold detection using 1 out of 8.

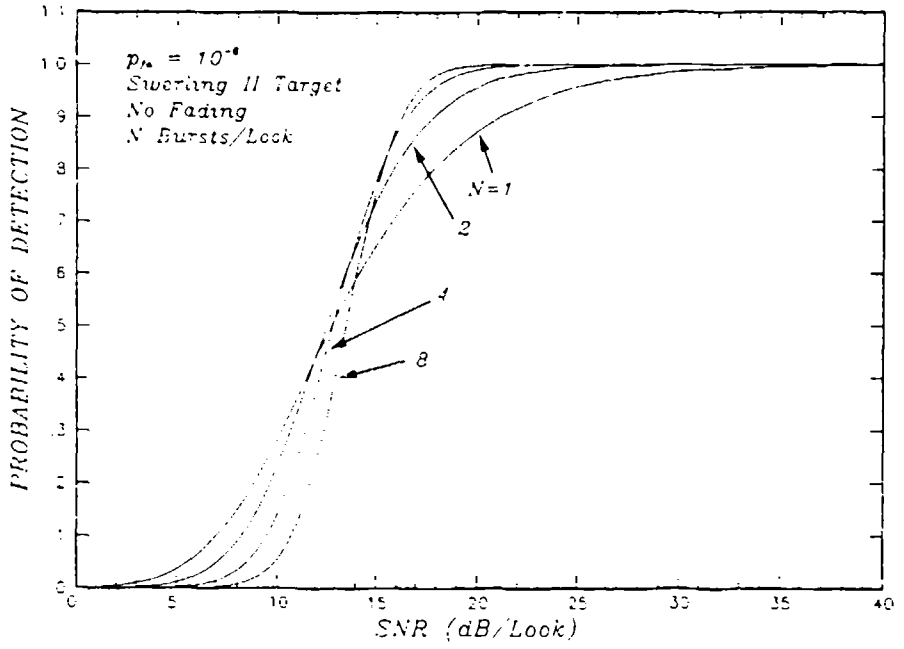

Figure 28. Probability of detecting a Swerling II target using noncoherent integration of bursts with no fading.

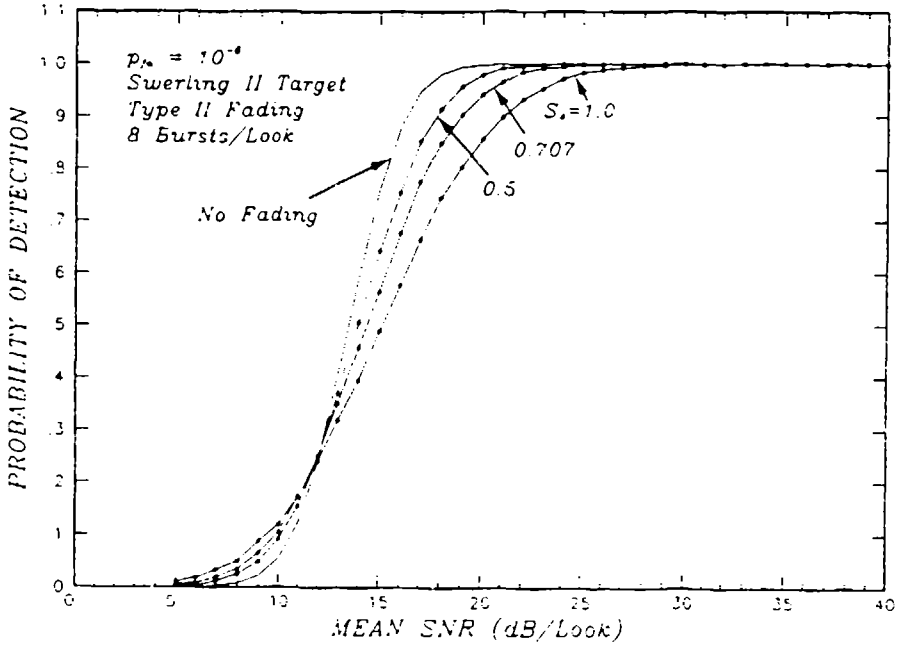

Figure 29. Probability of detecting a Swerling II target using noncoherent integration of 8 bursts during Type II Fading.

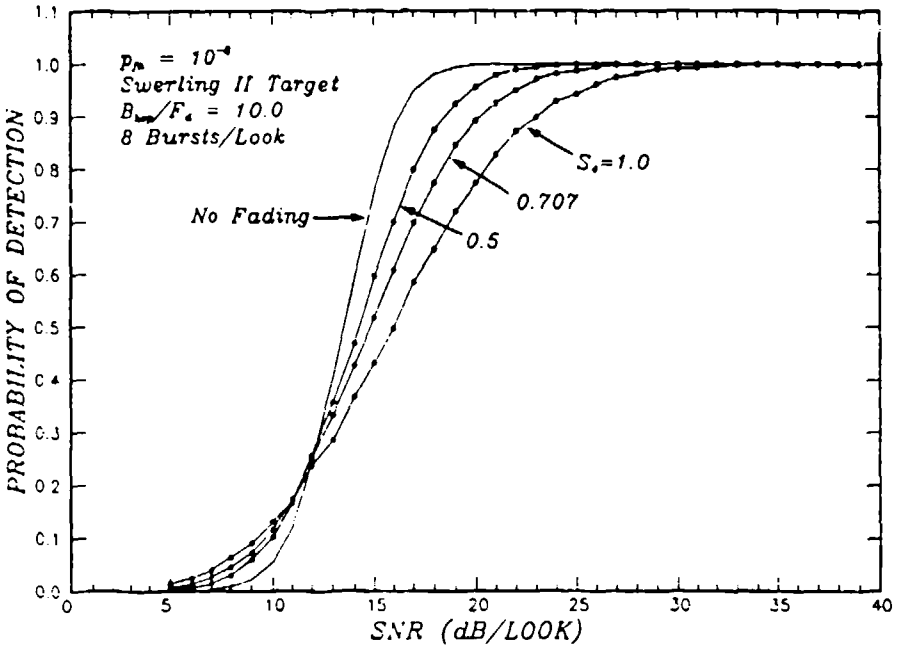

Figure 30. Probability of detecting a Swerling II target using noncoherent integration of 8 bursts for various scintillation levels assuming Gaussian correlation of bursts, $B_{hop}/f_d = 10$.

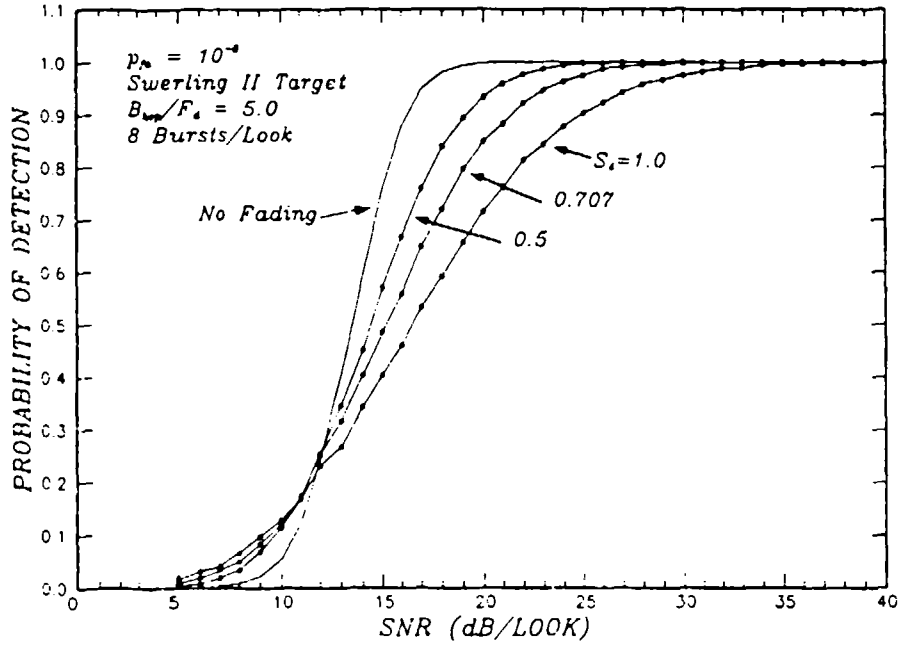

Figure 31. Probability of detecting a Swerling II target using noncoherent integration of 8 bursts for various scintillation levels assuming Gaussian correlation of bursts, $B_{hop}/f_d = 5$.

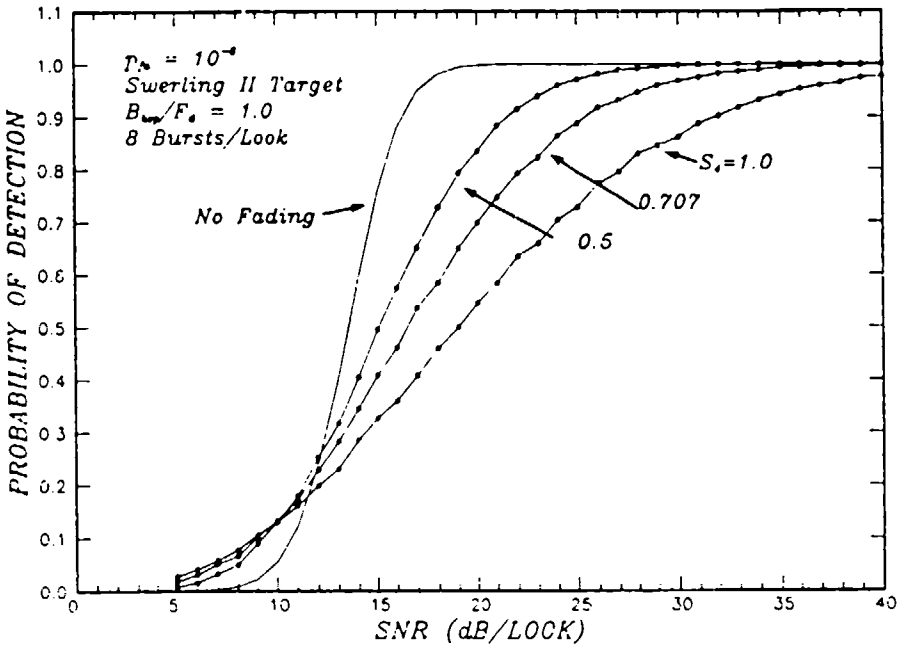

Figure 32. Probability of detecting a Swerling II target using noncoherent integration of 8 bursts for various scintillation levels assuming Gaussian correlation of bursts, $B_{hop}/f_d = 1$.

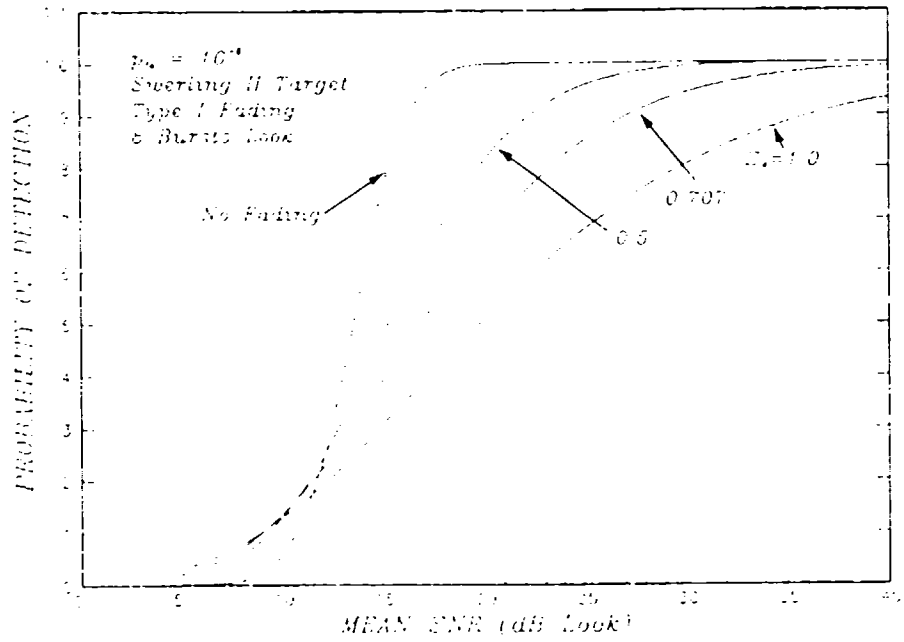

Figure 33. Probability of detecting a Swerling II target using noncoherent integration of 8 bursts during Type I Fading.

Figure 33 shows detection performance using 8 bursts per look in a Type I fading environment where the propagation effects on all bursts in a look are perfectly correlated. A comparison of this figure with Figure 20 again gives an advantage of about 2 dB relative to double threshold detection using 8 bursts per look.

SECTION 6

CONCLUSIONS

Severe fading has a strong effect on the target detection performance of a space based radar. In this report both analytic and simulation results for the performance of double threshold detection are compared to that of noncoherent integration of the returns from multiple bursts per look. Quantitative graphical results are given for various levels of scintillation severity ranging from no scintillation to worst case Rayleigh fading on the one-way propagation path. In addition, the effects of various amounts of correlation between the bursts in a look are considered through the use of Monte Carlo simulation techniques. For this work a simple Gaussian correlation function is used to specify frequency correlation of bursts for a frequency hopping radar. However, the simulation allows for an arbitrary correlation in frequency and in time between the radar returns from bursts in a look as long as the 'slow fading' assumption is not violated.

For a nonfluctuating target and worst-case fading, some gain is available through the M out of N combining process. However, as the level of scintillation decreases to less severe fluctuations, burst combining should be avoided since better performance is possible with a single burst. For a Swerling II target, both double threshold detection and noncoherent integration of multiple bursts per look offer some mitigation of the effects of fading, depending upon the severity of the fluctuations and on the correlation properties of the bursts of a look.

For the case of greatest interest here, the combining of 8 bursts to form a look, there is a gain of about 1.5 to 2 dB in detection sensitivity for noncoherent integration in comparison to double threshold detection. This conclusion is based on detection performance alone and does not consider any burst scheduling advantages of M out of N detection.

In order to apply the results for detection performance given in this report to help design a space based radar, it is necessary to obtain the value of the scintillation index as a function of radar transmission frequency, geometry, ionospheric conditions and time of day. The WBMOD computer code [*Fremouw and Secan*, 1984] contains the only world-wide model that gives this result. Work currently in progress at MRC involves the incorporation of a model of the probability density function for electron density fluctuations into WBMOD. This probability density function is necessary to

answer questions regarding the percent of time that the scintillation index is above or below any specific value and is, therefore, necessary to measure radar performance.

SECTION 7

REFERENCES

Aarons, J., "Global Morphology of Ionospheric Scintillation II," AFCRL-TR-75-0135, Air Force Cambridge Research Laboratories, 11 March 1975.

Arendt, P.R., and H. Soicher, "Effects of Arctic Nuclear Explosions on Satellite Radio Communication", *Proc. IEEE*, Vol. 52, pp. 672-676, June 1964.

Basu, Sunanda and S. Basu, "Correlated Measurements of Scintillations and In-Situ F-region Irregularities from 0go-6", *Geophys. Res. Lett.*, Vol. 3, pp. 681-684, 1976.

Budden, K. G., "The propagation of radio waves," Cambridge University Press, 1985.

Dana, R. A., and D. L. Knepp, "The Impact of Strong Scintillation on Space Based Radar Design I: Coherent Detection", *IEEE Transactions on Aerospace and Electronic Systems*, AES-19, No. 4, pp. 539-549, July 1983.

Dana, R. A., and D. L. Knepp, "The Impact of Strong Scintillation on Space Based Radar Design II: Noncoherent Detection", *IEEE Transactions on Aerospace and Electronic Systems*, Vol. AES-22, No. 1, pp. 34-46, January 1986.

Feller, W., *An Introduction to Probability Theory and Its Applications*, Vol. 1, New York, Wiley, 1957.

Franke, S. J., C. H. Liu and D. J. Fang, "Multifrequency Study of Ionospheric Scintillation at Ascension Island", *Radio Science*, Vol. 19, pp. 695-706, May-June 1984.

Fremouw, E. J., R. L. Leadabrand, R. C. Livingston, M. D. Cousins, C. L. Rino, B. C. Fair, and R. A. Long, "Early Results from the DNA Wideband Satellite Experiment", *Radio Science*, Vol. 13, pp. 167-187, January- February 1978.

Fremouw, E. J., R. C. Livingston and D. A. Miller, "On the Statistics of Scintillating Signals", *Journal of Atmospheric and Terrestrial Physics*, Vol. 42, pp. 717-731, 1980.

Fremouw, E. J. and J. Secan, "Modeling and Scientific Application of Scintillation Results," *Radio Science*, Vol. 18, pp. 687-694, May-June 1984.

Hawkins, G. and J. Mulien, "Daytime Equatorial Scintillations in VHF Trans-ionospheric Radio Wave Propagation from ATS-3 at Huancayo, Peru," URSI, Boulder, CO, 1974.

Hurst, R. L. and R. E. Knop, "Generation of Random Correlated Variables", *Comm ACM*, pp. 355-357, May 1972.

Keskinen, M. J. and S. L. Ossakow, "On the spatial power spectrum of the $\bar{E}$ X $\bar{B}$ gradient drift instability in ionospheric plasma clouds", *Geophys. Res.*, Vol. 86, p. 6947, 1981.

Knepp, D. L., "Aperture Antenna Effects After Propagation Through Strongly Disturbed Random Media", *IEEE Transactions on Antennas and Propagation*, Vol. AP-33, No. 10, pp. 1074-1084, October 1985.

Knepp, D. L. and G. C. Valley, "Properties of Joint Gaussian Statistics", *Radio Science*, Vol. 13, No. 1, pp. 59-68, January-February 1978.

King, M. A. and P. B. Fleming, "An Overview of the Effects of Nuclear Weapons on Communications Capabilities", *Signal*, pp. 59-66, January 1980.

Lawrence, R. S., C. G. Little, and H. J. A. Chivers, "A Survey of Ionospheric Effects Upon Earth-Space Radio Propagation," *Proc. IEEE*, Vol. 52, pp. 4-27, January 1964 (U).

Linder, I. W. and P. Swerling, "Performance of the Double-Threshold Radar Receiver in the Presence of Interference", ASTIA Doc. AD-11366, May 1956.

Livingston, R. C., "Comparative Equatorial Scintillation Morphology – American and Pacific Sectors," DNA 4644T, SRI International, June 1978.

Marcum, J. L., *A Statistical Theory of Target Detection by Pulsed Radar: Mathematical Appendix*, RM-753, Rand Corporation, July 1948.

Nakagami, M., The *m*-distribution - A General Formula of Intensity Distribution of Rapid Fading, in *Statistical Methods in Radio Propagation*, edited by W. C. Hoffman, pp. 3-36, Pergamon, New York, 1960.

Papoulis, A., *Probability, Random Variables, and Stochastic Processes*, New York, McGraw-Hill, 1965.

Schwartz, M., "A Coincidence Procedure for Signal Detection", *IRE Trans. Information Theory*, Vol. IT-2, pp. 135-139, December 1956.

Skinner, N. J., R. F. Kelleher, J. B. Hacking and C. W. Benson, "Scintillation Fading of Signals in the SHF Band", *Nature (Phys. Sci.)*, Vol. 232, pp. 19-21, July 1971.

Taur, R. R., "Simultaneous 1.5 and 4-GHz Ionospheric Scintillation Measurement", *Radio Science*, Vol. 11, pp. 1029-1036, December 1976.

Towle, D. M., "VHF and UHF Radar Observations of Equatorial *F* Region Ionospheric Irregularities and Background Densities", *Radio Science*, Vol. 15, No. 1, pp. 71-86, January-February 1980.

Tsunoda, R. T., "High-Latitude F-Region Irregularities: A Review and Synthesis", to appear in *Rev. Geophys.* in 1988.

Walker, J. F., "Performance Data for a Double-Threshold Detection Radar", *IEEE Transactions on Aerospace and Electronic Systems*, Vol. AES- 7, No. 1, pp. 142-146, January 1971.

Wolcott, J. H., D. J. Simons, T. E. Eastman, and T. J. Fitzgerald, "Characteristics of Late-Time Striations Observed During Operation STRESS", *Effect of the Ionosphere on Space and Terrestrial Systems*, J. M. Goodman, Ed., U. S. Government Printing Office, pp. 602-613, 1978.

DISTRIBUTION LIST

DNA-TR-89-82

DEPARTMENT OF DEFENSE

US NUC CMD & CENTRAL SYST SUPPORT STAFF
ATTN: SAB H SEQUINE

ASSISTANT TO THE SECRETARY OF DEFENSE ATOMIC ENERGY
ATTN: EXECUTIVE ASSISTANT

DEFENSE ADVANCED RSCH PROJ AGENCY
ATTN: CHIEF SCIENTIST
ATTN: GSD R ALEWINE

DEFENSE COMMUNICATIONS AGENCY
ATTN: A320
ATTN: DR P CROWLEY

DEFENSE COMMUNICATIONS ENGINEER CENTER
ATTN: CODE R410

DEFENSE INTELLIGENCE AGENCY
ATTN: DB-TPO
ATTN: DC-6
ATTN: DIR
ATTN: DT-1B
ATTN: RTS-2B

DEFENSE NUCLEAR AGENCY
ATTN: DFSP G ULLRICH
ATTN: NANF
ATTN: NASF
ATTN: OPNA
3 CYS ATTN: RAAE
ATTN: RAAE A CHESLEY
ATTN: RAAE A MARDIGUIAN
ATTN: RAAE G ULLRICH
ATTN: RAAE M CRAWFORD
ATTN: RAAE S BERGGREN
ATTN: RAEE
4 CYS ATTN: TITL

DEFENSE NUCLEAR AGENCY
ATTN: TDNM
2 CYS ATTN: TDTT W SUMMA

DEFENSE TECHNICAL INFORMATION CENTER
2 CYS ATTN: DTIC/FDAB

JOINT DATA SYSTEM SUPPORT CTR
ATTN: C-312

JOINT STRAT TGT PLANNING STAFF
ATTN: JKC (ATTN: DNA REP)
ATTN: JKCS, STUKMILLER
ATTN: JLWT (THREAT ANALYSIS)
ATTN: JPEM
ATTN: JPSS

NATIONAL SECURITY AGENCY
ATTN: C GOEDEKE

STRATEGIC AND THEATER NUCLEAR FORCES
ATTN: DR E SEVIN
ATTN: DR SCHNEITER
ATTN: LC R DAWSON

STRATEGIC DEFENSE INITIATIVE ORGANIZATION
ATTN: EN
ATTN: EN LTC C JOHNSON
ATTN: PTN C GIESE
ATTN: PTP LTC SEIBERLING
ATTN: TN

THE JOINT STAFF
ATTN: J6

DEPARTMENT OF THE ARMY

ARMY LOGISTICS MANAGEMENT CTR
ATTN: DLSIE

HARRY DIAMOND LABORATORIES
ATTN: SLCIS-IM-TL (TECH LIB)

U S ARMY ATMOSPHERIC SCIENCES LAB
ATTN: DR F NILES
ATTN: SLCAS-AE-E
ATTN: SLCAS-AR DR H HOLT

U S ARMY COMMUNICATIONS R&D COMMAND
ATTN: AMSEL-RD-ESA

U S ARMY FOREIGN SCIENCE & TECH CTR
ATTN: DRXST-SD

U S ARMY MISSILE COMMAND/AMSMI-RD-CS-R
ATTN: AMSMI-RD-CS-R (DOCS)

U S ARMY NUCLEAR & CHEMICAL AGENCY
ATTN: MONA-NU

U S ARMY NUCLEAR EFFECTS LABORATORY
ATTN: ATAA-PL
ATTN: ATAA-TDC
ATTN: ATRC-WCC

U S ARMY STRATEGIC DEFENSE CMD
ATTN: CSSD-H-LS B CARRUTH
ATTN: CSSD-H-SA
ATTN: CSSD-H-SA/R SMITH
ATTN: CSSD-H-SAV
ATTN: CSSD-H-TT M POPE

U S ARMY STRATEGIC DEFENSE COMMAND
ATTN: BMDATC-R W DICKERSON

USA SURVIVABILITY MANAGMENT OFFICE
ATTN: SLCSM SE J BRAND

DEPARTMENT OF THE NAVY

COMMAND & CONTROL PROGRAMS
ATTN: OP 941

JOINT CRUISE MISSILES PROJECT OFC (PM-3)
ATTN: JCMG-707

NAVAL AIR SYSTEMS COMMAND
ATTN: PMA 271

NAVAL ELECTRONICS ENGRG ACTVY, PACIFIC
ATTN: CODE 250 D OBRYHIM

NAVAL RESEARCH LABORATORY
ATTN: CODE 2000 J BROWN
ATTN: CODE 2627 (TECH LIB)
2 CYS ATTN: CODE 4100 H GURSKY
ATTN: CODE 4121.8 H HECKATHORN
ATTN: CODE 4183
ATTN: CODE 4701
ATTN: CODE 4720 J DAVIS
ATTN: CODE 4750 P RODRIGUEZ
ATTN: CODE 4780 B RIPIN
ATTN: CODE 4780 DR P BERNHARDT
ATTN: CODE 4780 J HUBA
ATTN: CODE 5300
ATTN: CODE 5326 G A ANDREWS
ATTN: CODE 5340 E MOKOLE
ATTN: CODE 8344 M KAPLAN

NAVAL SURFACE WARFARE CENTER
ATTN: CODE H-21

NAVAL TECHNICAL INTELLIGENCE CTR
ATTN: DA44

NAVAL UNDERWATER SYSTEMS CENTER
ATTN: CODE 3411, J KATAN

OFC OF THE DEPUTY CHIEF OF NAVAL OPS
ATTN: OP 654
ATTN: OP 941D
ATTN: OP 981N

SPACE & NAVAL WARFARE SYSTEMS CMD
ATTN: CODE 3101 T HUGHES
ATTN: PD 50TD
ATTN: PD50TD1 G BRUNHART
ATTN: PME 106-4 S KEARNEY
ATTN: PME 106 F W DIEDERICH

THEATER NUCLEAR WARFARE PROGRAM OFC
ATTN: PMS-42331F (D SMITH)

DEPARTMENT OF THE AIR FORCE

AFIA
ATTN: AFIA/INKD MAJ SCHROCK

AIR FORCE CTR FOR STUDIES & ANALYSIS
ATTN: AFCSA/SASC

AIR FORCE ELECTRONIC WARFARE CENTER
ATTN: LT M MCNEELY

AIR FORCE GEOPHYSICS LABORATORY
ATTN: J KLOUBACHAR
ATTN: OP/W BLUMBERG
ATTN: SANTI BASU
ATTN: SUL

AIR FORCE SPACE SYSTEMS DIVISION
ATTN: YA
2 CYS ATTN: YN

AIR UNIVERSITY LIBRARY
ATTN: AUL-LSE

HQ AWS, DET 3 (CSTC/WE)
ATTN: WE

STRATEGIC AIR COMMAND/XRFS
ATTN: XRFS

WEAPONS LABORATORY
ATTN: NTCA
ATTN: NTN
ATTN: SUL

DEPARTMENT OF ENERGY

EG&G, INC
ATTN: D WRIGHT

LAWRENCE LIVERMORE NATIONAL LAB
ATTN: L-97 T DONICH

LOS ALAMOS NATIONAL LABORATORY
ATTN: D SAPPENFIELD
ATTN: D WINSKE

SANDIA NATIONAL LABORATORIES
ATTN: D HARTLEY

SANDIA NATIONAL LABORATORIES
ATTN: A D THORNBROUGH
ATTN: C S WILLIAMS
ATTN: CODE 9014 R BACKSTROM
ATTN: D DAHLGREN
ATTN: ORG 9114 W D BROWN
ATTN: SPACE PROJECT DIV
ATTN: TECH LIB

OTHER GOVERNMENT

CENTRAL INTELLIGENCE AGENCY
ATTN: OSWR/NED
ATTN: OSWR/SSD FOR L BERG

DEPARTMENT OF COMMERCE
ATTN: E MORRISON
ATTN: G REEVE
ATTN: J HOFFMEYER
ATTN: W UTLAUT

U S DEPARTMENT OF STATE
ATTN: PM/TMP

DEPARTMENT OF DEFENSE CONTRACTORS

AEROSPACE CORP
ATTN: A MORSE
ATTN: B P PURCELL
ATTN: C CREWS
ATTN: C RICE
ATTN: G LIGHT
ATTN: I GARFUNKEL
ATTN: J KLUCK
ATTN: M ROLENZ

ANALYTICAL SYSTEMS ENGINEERING CORP
ATTN: SECURITY

ATLANTIC RESEARCH SERVICES CORP
ATTN: R MCMILLAN

ATMOSPHERIC AND ENVIRONMENTAL RESEARCH INC
ATTN: M KO

AUSTIN RESEARCH ASSOCIATES
ATTN J THOMPSON

AUTOMETRIC INCORPORATED
ATTN C LUCAS

BDM INTERNATIONAL INC
ATTN L JACOBS

BERKELEY RSCH ASSOCIATES, INC
ATTN J WORKMAN
ATTN N T GLADD
ATTN S BRECHT

BOEING CO
ATTN G HALL

CALIFORNIA RESEARCH & TECHNOLOGY, INC
ATTN M ROSENBLATT

CHARLES STARK DRAPER LAB, INC
ATTN A TETEWSKI

COMMUNICATIONS SATELLITE CORP
ATTN G HYDE

CORNELL UNIVERSITY
ATTN D FARLEY JR
ATTN M KELLY

ELECTROSPACE SYSTEMS, INC
ATTN P PHILLIPS

EOS TECHNOLOGIES, INC
ATTN B GABBARD
ATTN R LELEVIER

GENERAL ELECTRIC CO
ATTN ROBERT H EDSALL

GENERAL RESEARCH CORP INC
ATTN J EOLL

GRUMMAN AEROSPACE CORP
ATTN J DIGLIO

HSS, INC
ATTN D HANSEN

INFORMATION SCIENCE, INC
ATTN W DUDZIAK

INSTITUTE FOR DEFENSE ANALYSES
ATTN E BAUER
ATTN H WOLFHARD

J S LEE ASSOCIATES INC
ATTN DR J LEE

JAYCOR
ATTN J SPERLING

JOHNS HOPKINS UNIVERSITY
ATTN C MENG
ATTN J D PHILLIPS
ATTN R STOKES
ATTN T EVANS

KAMAN SCIENCES CORP
ATTN DASIAC
ATTN E CONRAD
ATTN G DITTBERNER

KAMAN SCIENCES CORPORATION
ATTN B GAMBILL
ATTN DASIAC
ATTN R RUTHERFORD

LOCKHEED MISSILES & SPACE CO, INC
ATTN J HENLEY
ATTN J KUMER
ATTN R SEARS

LOCKHEED MISSILES & SPACE CO, INC
ATTN D KREJCI
ATTN D T RAMPTON

LTV AEROSPACE & DEFENSE COMPANY
2 CYS ATTN LIBRARY

M I T LINCOLN LAB
ATTN D TOWLE
ATTN I KUPIEC
ATTN M LEE

MARTIN MARIETTA DENVER AEROSPACE
ATTN H VON STRUVE III
ATTN J BENNETT

MAXIM TECHNOLOGIES, INC
ATTN B RIDGEWAY
ATTN J SCHLOBOHM

MCDONNELL DOUGLAS CORPORATION
ATTN J GROSSMAN
ATTN R HALPRIN

METATECH CORPORATION
ATTN R SCHAEFER
ATTN W RADASKY

METEOR COMMUNICATIONS CORP
ATTN R LEADER

MISSION RESEARCH CORP
ATTN R ARMSTRONG
ATTN W WHITE

MISSION RESEARCH CORP
ATTN B R MILNER
ATTN C LONGMIRE
ATTN D ARCHER
2 CYS ATTN D KNEPP
ATTN D LANDMAN
ATTN F FAJEN
ATTN F GUIGLIANO
ATTN G MCCARTOR
2 CYS ATTN J T REINKING
2 CYS ATTN J TODD
ATTN K COSNER
ATTN M FIRESTONE
ATTN R BIGONI
ATTN R BOGUSCH
ATTN R DANA

ATTN: R HENDRICK
ATTN: R KILB
ATTN: S GUTSCHE
ATTN: TECH INFO CENTER
ATTN: TECH LIBRARY

MITRE CORPORATION
ATTN: M HORROCKS
ATTN: R C PESCI
ATTN: W FOSTER

NORTHWEST RESEARCH ASSOC, INC
ATTN: E FREMOUW

PACIFIC-SIERRA RESEARCH CORP
ATTN: E FIELD JR
ATTN: F THOMAS
ATTN: H BRODE

PHOTOMETRICS, INC
ATTN: I L KOFSKY

PHOTON RESEARCH ASSOCIATES
ATTN: D BURWELL
ATTN: O LEWIS

PHYSICAL RESEARCH INC
ATTN: W SHIH

PHYSICAL RESEARCH INC
ATTN: H FITZ
ATTN: W HEUSER

PHYSICAL RESEARCH, INC
ATTN: R DELIBERIS
ATTN: T STEPHENS

PHYSICAL RESEARCH, INC
ATTN: J DEVORE
ATTN: J THOMPSON
ATTN: W SCHLUETER

PHYSICS INTERNATIONAL CO
ATTN: C GILMAN

R & D ASSOCIATES
ATTN: C GREIFINGER
ATTN: F GILMORE
ATTN: G HOYT
ATTN: M GANTSWEG

RAND CORP
ATTN: C CRAIN
ATTN: E BEDROZIAN

RAND CORP
ATTN: B BENNETT

RJO ENTERPRISES/POET FAC
ATTN: A ALEXANDER
ATTN: W BURNS

SCIENCE APPLICATIONS INTL CORP
ATTN: S ROSENCWEIG

SCIENCE APPLICATIONS INTL CORP
ATTN: C SMITH
ATTN: D HAMLIN
ATTN: D SACHS
ATTN: L LINSON

SCIENCE APPLICATIONS INTL CORP
ATTN: D TELAGE
ATTN: M CROSS

SRI INTERNATIONAL
ATTN: R LIVINGSTON
ATTN: R T TSUNODA
ATTN: W CHESNUT
ATTN: W JAYE

STEWART RADIANCE LABORATORY
ATTN: R HUPPI

TELECOMMUNICATION SCIENCE ASSOCIATES
ATTN: R BUCKNER

TELEDYNE BROWN ENGINEERING
ATTN: J WOLFSBERGER, JR
ATTN: N PASSINO

TOYON RESEARCH CORP
ATTN: J ISE

TRW INC
ATTN: H CULVER

TRW SPACE & DEFENSE SYSTEMS
ATTN: D M LAYTON

USER SYSTEMS, INC
ATTN: S W MCCANDLESS, JR

UTAH STATE UNIVERSITY
ATTN: K BAKER
ATTN: L JENSEN

VISIDYNE, INC
ATTN: J CARPENTER

FOREIGN

FOA 2
ATTN: B SJOHOLM

FOA 3
ATTN: T KARLSSON

DIRECTORY OF OTHER

BOSTON UNIVERSITY
ATTN: MICHAEL MENDILLO